This is to certify that the

thesis entitled

EXPLORATORY INVESTIGATION OF THE RECIRCULATION
REGION AND SEARCH FOR COHERENT MOTIONS AFT OF
AN AXIALLY MOUNTED CONE IN CONFINED FLOW

presented by

Cherie Michele Laws Holland

has been accepted towards fulfillment
of the requirements for

Master of Science degree in Mechanical Engineering

_____
Major professor

Date 24 April 1989

PLACE IN RETURN BOX to remove this checkout from your record.
TO AVOID FINES return on or before date due.

DATE DUE	DATE DUE	DATE DUE
JAN 1 1 2009 010310		

EXPLORATORY INVESTIGATION OF THE RECIRCULATION REGION

AND SEARCH FOR COHERENT MOTIONS

AFT OF AN AXIALLY MOUNTED CONE

IN CONFINED FLOW

By

Cherie Michele Laws Holland

A THESIS

Submitted to
Michigan State University
in partial fulfillment of the requirements
for the degree of

MASTER OF SCIENCE

Department of Mechanical Engineering

1989

ABSTRACT

EXPLORATORY INVESTIGATION OF THE RECIRCULATION REGION AND SEARCH FOR COHERENT MOTIONS AFT OF AN AXIALLY MOUNTED CONE IN CONFINED FLOW

By

Cherie Michele Laws Holland

The wake flow aft of a centered conical obstruction in confined flow - a geometry which simulates that of a flame stabilizer - was investigated for the purpose of i) detecting the presence of large-scale coherent motions, and ii) characterizing some of the features of the recirculation region. Two cones, representing blockage ratios of 0.20 and 0.50, were employed to compare the influence of the flow geometry on characteristics such as strength and frequency of any observed coherent motions and the length and the maximum cross sectional area of the recirculation region. Time series measurements of the velocity fluctuations in the irrotational flow were used for the detection of coherent motions. Static pressure profiles, surface streaking on the cone, and hot-wire detection of the vortical fluid near the separation stream surface were used to characterize some of the features of the recirculation region. The results of this investigation reveal no evidence of large-scale coherent motions. Several properties of the recirculation region have been quantitatively identified by these measurements.

ACKNOWLEDGMENTS

ACKNOWLEDGMENTS (cont'd)

TABLE OF CONTENTS

LIST OF TABLES

LIST OF FIGURES

NOMENCLATURE

A	annular cross sectional area
c_p	pressure coefficient
d	diameter of cone base
E	voltage
f	frequency
l_i	integral length scale
N	node
n	statistically independent samples
p	pressure
R	radius of confining tube
r	radial displacement
Re	Reynold's number
S	saddle
s	number of samples
St	Strouhal number
t_c	convective length time scale
U	velocity
w	radius of largest cross sectional area of recirculation region
X	Euler characteristic of a surface
x	axial (streamwise) displacement
λ	wavelength
σ	standard deviation of a population

NOMENCLATURE (cont'd)

Σ	sum; summation
μ	uncertainty in the mean value of a population
θ	angular displacement
ρ	density

1. INTRODUCTION

Characterization of the recirculating flow aft of a flame stabilizer aids in the understanding of flow features such as flame stability and processes such as the exchange of mass and energy. The wake flow aft of a centered conical obstruction in confined flow - a geometry which simulates that of a flame stabilizer - is recognized to contain a wide range of scales in its turbulent motion. Those motions which are both large and coherent will most readily reveal their presence in the correlated velocity fluctuations of the irrotational annular flow between the wall boundary layer and the central wake. The primary purpose of the present investigation is the search for the presence of such motions with a secondary purpose being the characterization of some of the features of the recirculation region.

It is well established that bluff bodies can exhibit vortex shedding at a predominant frequency. In studies of a two-dimensional flame holder geometry, Fujii, Gomi, and Eguchi (1978) and Fujii and Eguchi (1981), detected predominant frequencies in the velocity fluctuations within and outside of the recirculation region. Kamemoto, Oda, and Aizawa (1984) investigated the flow around a cylinder of triangular cross section (of width h) near a plane surface acting as a confining wall on one side. They related the frequency of vortex shedding from the cylinder to the gap distance, g, from the plane surface and found that regular vortex shedding was suppressed at a gap distance of less than about $g/h = 0.37$.

1

In three-dimensional, unconfined wake flows, several investigators have reported vortex shedding behavior. In studying the near wake properties of axisymmetric bluff body flows, Humphries and Vincent (1976, p. 658) generalized that,"in all bluff body flows there is a spectrum of turbulence in the wake shear layers which has a peak frequency, the shedding frequency, at which fluid is entrained from the wake bubble more strongly than at other frequencies." In a study by Calvert (1967) the wakes of cones and disks supported by a downstream sting show a definite periodicity at a predominant frequency. Durao and Whitelaw (1978) detected predominant frequencies in the axial and radial velocity components associated with the outer shear layer of an annular jet with a center body truncated at the exit plane. The ratio of the center body diameter to diameter of nozzle outlet ranged from 0.45 to 0.71 in that study. Their geometry is depicted in Figure 1.1. No dominant frequencies were observed within the wake recirculation region. In a study of an annular jet with a geometry similar to that of Figure 1.1 (center body resembling a cylinder truncated at the exit plane), Lam, Ko, and Lau (1986) observed vortex shedding of a predominant frequency from the wake region aft of the center body (body diameter to nozzle diameter was 0.45). The dynamics of the observed coherent motions in the wake were described using a processing technique developed by Fuchs, Mercker, and Michel (1979). Durao and Firmino (1984) detected the presence of predominant oscillations of the axial velocity component in
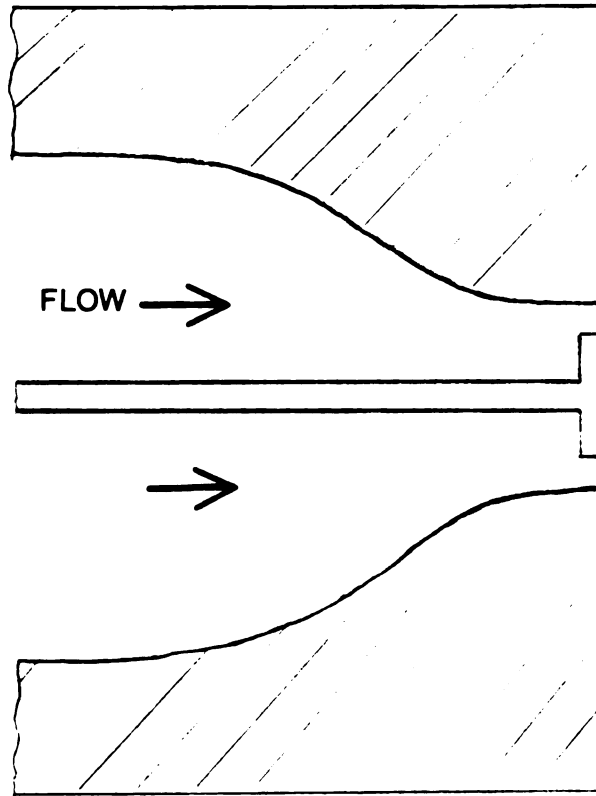
FLOW

Figure 1.1 Geometry of Annular Jet with Truncated Center
Body (Durao and Whitelaw [1978]).

the outer edges of the wake flow aft of disks and cones located on the centerline of a jet approximately 1 to 7 body diameters downstream of the exit plane. In a similar study, Fuchs et al (1979) detected periodic fluctuations at a predominant frequency in the flow aft of a disk in an open jet wind tunnel. They developed a processing technique in which a narrow band-pass filtered cross spectrum function was used to describe the azimuthal coherence properties of the irrotational velocity fluctuations. With this technique they were able to decompose the observed large-scale motions into a combination of relatively simple modes. This type of processing was also used by Xia and Bearman (1983) to describe the large-scale motions behind a bluff body with an axisymmetric fore-body and a slanted base.

In three-dimensional, confined wake flows similar to those existing in flame stabilizers, the reports of periodicity are varied. Using an optical technique involving a flame photometer, Winterfeld (1965) observed low frequency flow fluctuations throughout the recirculation region and periodic fluctuations of the boundary layer of the recirculation region for an axisymmetric flame holder geometry with blockage ratios of 0.04 to 0.36. However, in a study of disks with blockage ratios of 0.25 and 0.50 and a cone with a blockage ratio of 0.25 supported by an upstream sting, Taylor and Whitelaw (1984) observed no vortex shedding at any predominant frequency. A check for vortex shedding was performed using power spectra of the axial velocity fluctuations and a flow visualization technique.

Taylor and Whitelaw also compiled results from previous studies on recirculation region characteristics such as their lengths and cross sectional radii at the widest locations.

The present investigation was conducted in an axisymmetric, confined flow field simulating that of a cone shaped flame stabilizer. The geometry has a centered conical bluff body confined by a pipe with blockage ratios of 0.20 and 0.50. Hot-wire probe time series measurements of the velocity fluctuations in the irrotational flow were performed to detect the presence of any wake periodicity or large-scale coherent motions. Static pressure profiles, a surface streaking study on the cone, and hot-wire probe detection of the vortical fluid generated near the separation stream surface were performed to characterize some features of the recirculation region and check for disturbances caused by the probe holding apparatus. The two blockage ratios were chosen to allow comparison of the influence of the flow geometry on characteristics such as strength and frequency of any observed coherent motions and the length and cross sectional areas of the recirculation region. An array of four hot-wire probes was located in the irrotational flow between the separation stream surface and wall boundary layers to provide the time series information. The investigation was conducted at the LSTM-Erlangen (School for Fluid Mechanics of Erlangen) in West Germany.

The following section contains an analysis of the types of information to be expected from the static pressure

profiles, the one-point laser-Doppler anemometer (LDA) measurement, and the power spectra of the hot-wire time series data. A detailed description of the experimental equipment and flow system is given in Section 3.. The data acquisition and processing procedures are described in Section 4.. Section 5. contains the results of the present investigation and their interpretation. The conclusions of the investigation are presented in Section 6..

2. GENERAL CONSIDERATIONS OF THE DATA

A discussion of the data collected in the present investigation is presented in the following three subsections. An interpretation of the static pressure profile data is presented in Subsection 2.1.. Subsection 2.2. contains an analysis of the information from the one-point LDA measurements. An analysis of the information obtained from the spectral results is contained in Subsection 2.3..

2.1. Interpretation of Static Pressure Data

The pressure taps in the wall of the measuring section provide the static pressure in the flowing fluid if the streamlines are parallel to the wall. The pressure profile along the length of the pipe provides information on the shape of the separation stream surface aft of the cone; the most negative pressure values correspond to areas where the flow is most constricted, or equivalently, where the magnitude of flow velocity is the largest. In the flow geometry of the present investigation, this would occur at the point where the recirculation region aft of the cone has the greatest cross sectional area.

The static pressure profile data can also provide information about the effect of the hot-wire probe holding apparatus on the pressure field in the measuring section. A quantitative comparison of the static pressure profiles performed with and without the probe holding apparatus in the measuring section can be made using a pressure

7

coefficient defined as

$$c_p = \frac{p_{plenum} - p(x)}{p_{plenum} - p_{inlet}} \qquad (2.1)$$

where p_{plenum} is the pressure in the upper plenum, p_{inlet} is the pressure at the inlet of the measuring section, and $p(x)$ is the pressure at the measurement location.

2.2. Interpretation of the LDA Measurements

One-point LDA measurements of the axial velocity component (along the measuring section centerline, downstream of the cone) are used to provide information on the recirculation region. A LDA measurement using Bragg cell frequency shifting allows the direction of the mean velocity to be discerned. If the averaged mean velocity vector is directed upstream it is inferred that the measurement location is within the recirculation region.

The one-point LDA measurement also provides information about the effect of the hot-wire probe holding apparatus on the recirculation region. Similar to the procedure for the static pressure profiles, a one-point LDA measurement can be made with the probe-holding apparatus positioned in the measuring section and another measurement made after removing the apparatus while the wind tunnel is still operating. Removal of the probe holding apparatus causes a minimal (approximately 5 %) increase in the Reynolds number (based on diameter of measuring section) of the approach

flow. It is inferred that this minimal increase in the approach flow velocity does not produce a significant change in the flow field of the recirculation region. Measurements made near the close of the recirculation region should be sensitive to any changes in the flow field. A comparison of the averaged mean velocity at a point on the centerline axis of symmetry near this location should reveal any significant changes in the flow field of the recirculation region produced by the introduction of the probe-holding apparatus into the measuring section.

2.3. Interpretation of Spectral Results

A power spectral analysis of the hot-wire probe time series data serves as a diagnostic tool to detect the presence of periodic motions occuring at predominant frequencies. Spectral peaks can represent motions caused by such phenomena as vortex shedding at a predominant frequency, structural vibrations, and acoustic resonances. If large-scale coherent motions are present in a flow field, the data processing technique developed by Fuchs et al (1979) can be utilized to easily detect and describe these motions. The technique enables several different ways of characterizing turbulence in axisymmetric flows. For a comprehensive explanation of this technique, the reader is referenced to the investigation of Fuchs et al (1979).

3. EXPERIMENTAL EQUIPMENT

A detailed description of the experimental apparatus and instrumentation is presented in two main subsections. A description of the flow system and measuring section is given in Subsection 3.1.. Subsection 3.2. contains instrumentation information on the hot-wire and LDA systems.

3.1. Flow System

The construction and testing of the flow system was performed as part of the preparation for the present investigation. Details of this work are covered in the following two subsections. A brief synopsis of the fabrication procedure and a description of the wind tunnel are contained in Subsection 3.1.1.. A description of the measuring section is presented in Subsection 3.1.2..

3.1.1. Wind Tunnel

The flow system was a closed circuit wind tunnel that could provide a relatively large Reynolds number flow past the conical obstruction. A schematic representation of the tunnel, with dimensions, is given in Figure 3.1. Most of the flow system was housed in two prefabricated shipping containers that were converted into small laboratory rooms. The shell of the flow system was configured by placing one container atop the other, leaving an overhang to cover the blower which was placed at the rear of the lower container. The area around the blower was subsequently walled in, creating the side plenum. The floor between the side

UPPER PLENUM

6.0 m

3.0 m

Screen Box

support detail
in Figure 3.2

Baffle

LOWER PLENUM

3.0 m

SIDE
PLENUM

6.0 m

2.0 m
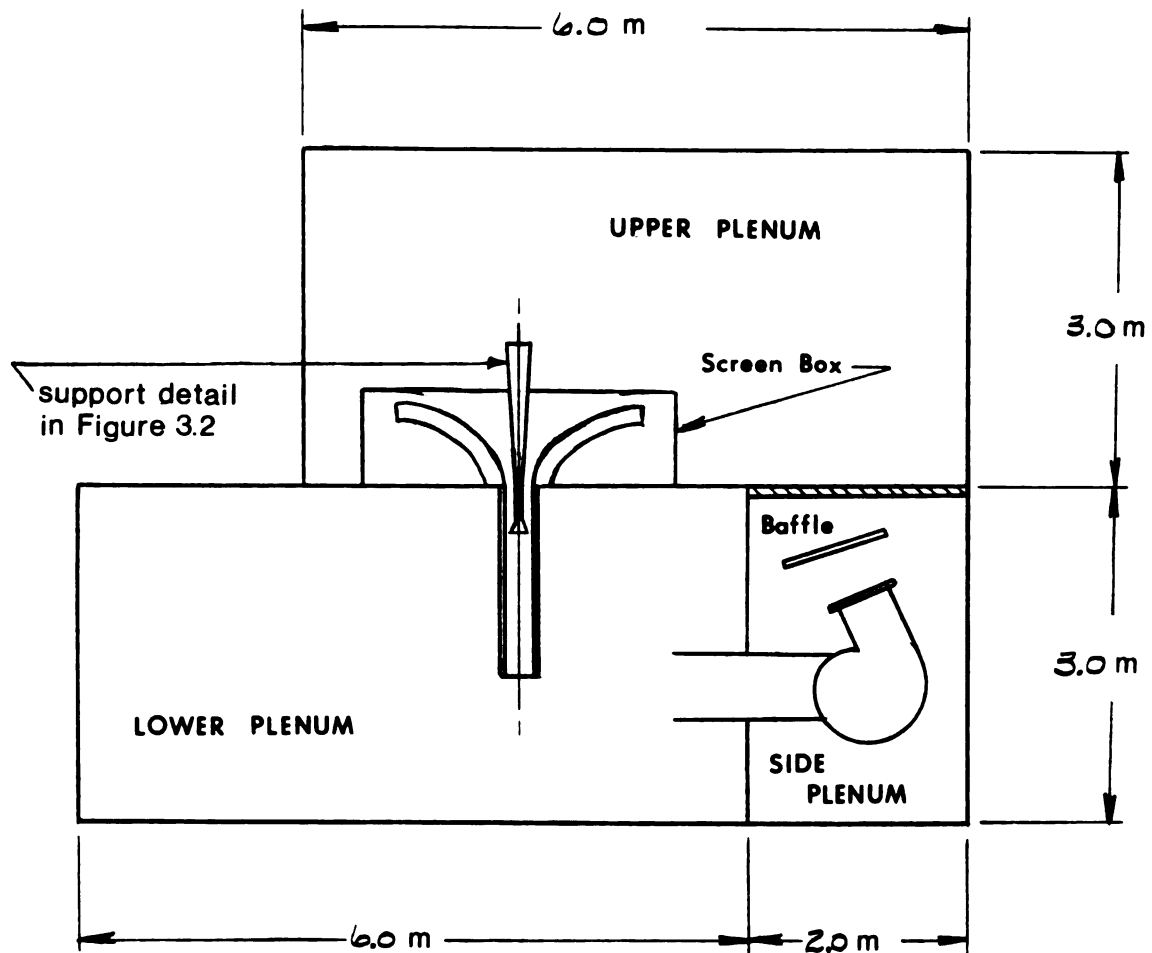
NOTE: Flow System
Depth is 2.5 m

Figure 3.1 Flow System.

plenum and upper plenum was removed to allow air circulation. The air intake for the blower was located in the lower plenum and the outlet exhausted towards the upper plenum. There was a metal baffle at the outlet of the blower which was used to speed the dissipation of the kinetic energy of the air entering the upper plenum.

The contraction was located between the upper plenum, which served as a settling chamber, and the lower plenum, which housed the measuring section. Two static pressure taps were provided, one in the upper plenum and one in the wall of the measuring section at the contraction outlet. There was also a thermocouple in the upper plenum to provide air temperature readings.

The contour of the contraction was calculated by choosing an appropriate non-dimensional stream function, as detailed by Smith and Wang (1944), that gives a throat speed distribution that is uniform (theoretically) within a fifth of one percent. For details of the calculations for the contraction, the reader is referenced to the publication by Smith and Wang (1944). The contraction ratio was 7.5:1 with a throat diameter of 200 mm. The contraction was formed from a series of wooden slabs of 25 mm thickness that were layered, glued together, and machined according to the contraction calculations.

A sting was centered inside the contraction and was used as a support for objects in the measuring section. Both the sting and contraction are schematically represented in Figure 3.2. The sting was turned from a single piece of

STING:
Contraction Ratio – 9:1

AXISYMMETRIC CONTRACTION:
Contraction Ratio – 7.5:1
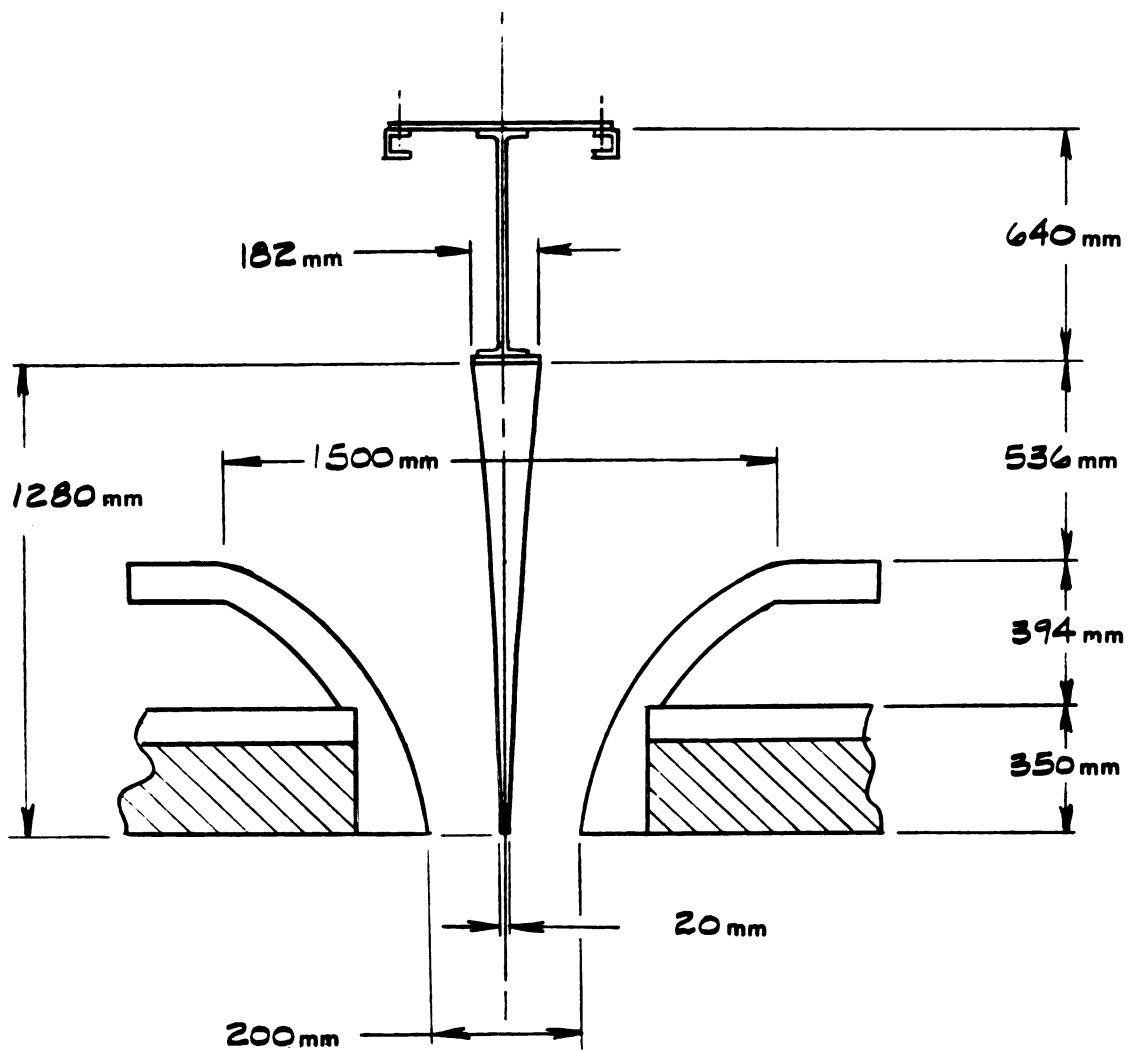
Figure 3.2   Contraction and Sting.

aluminum and had a contraction ratio of 9:1. The diameter at the throat of the sting was 20 mm as compared to 200 mm for the contraction at this location. The contour for the sting was calculated using a stream function similar to that of the contraction contour. The sting was anchored from the ceiling of the upper plenum with steel C-beams.

There were two types of turbulence manipulators in this flow system. The first type consisted of precision screen (30 mesh/inch) in tandem with a dense fiber filter material of 10 mm thickness. This combination was located in the 2000 mm x 2500 mm area between the side and upper plenums. The second type of turbulence manipulator was a screen (30 mesh/inch) configuration around the contraction inlet. To ensure that the air flow entering the contraction travelled through the screen, a welded steel frame that completely surrounded the contraction was built to support the screen sections. This screen box is shown in Figure 3.3.

3.1.2. Measuring Section

A removable plexiglass pipe piece mounted at the outlet of the axisymmetric contraction formed the measuring section. Pipe sections with various lengths, and some with pressure taps, were fabricated to afford a degree of flexibility in the length of the measuring section. The pipe sections were created from a sheet of plexiglass rolled to an inner diameter of 200 mm. The walls of the pipe sections were finely polished to allow the use of LDA measuring techniques. Details of the measuring section are shown in

830 mm

2140 mm

1100 mm

990 mm
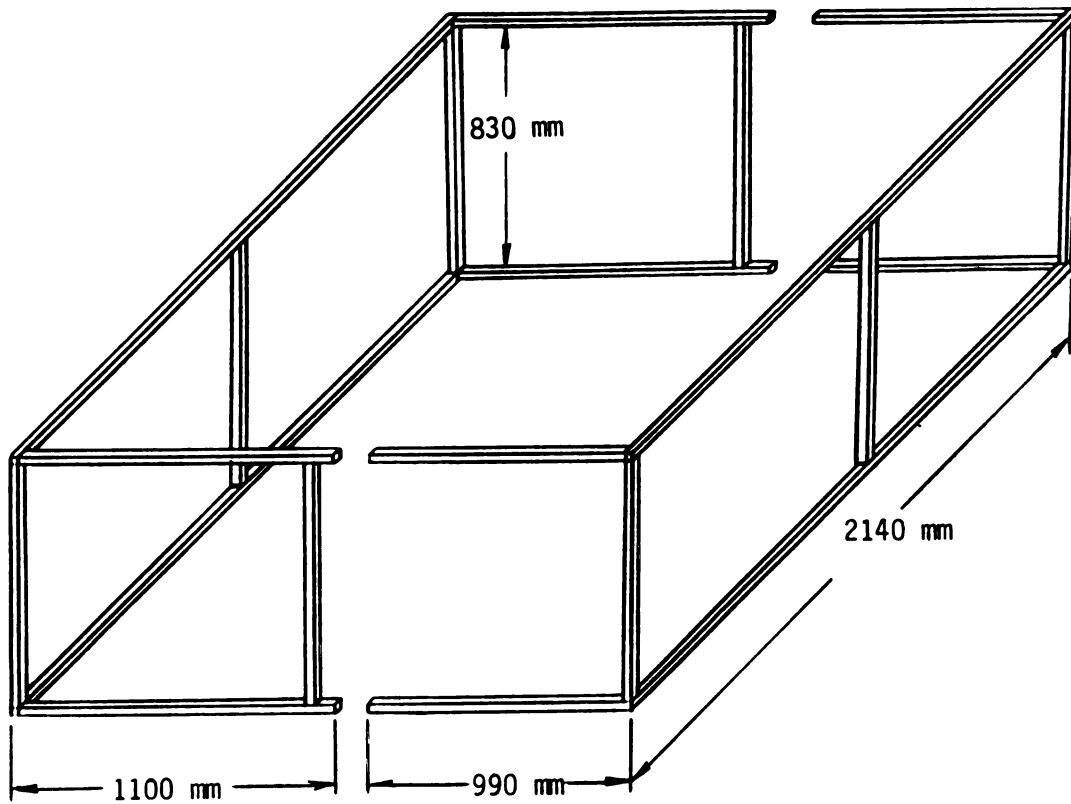
Note: screen covers frame
on all sides but
bottom

Figure 3.3 Screen Box Turbulence Manipulator.

Figure 3.4. A cone section supported by the upstream sting was centered along the axis of symmetry of the pipe. The cone section was comprised of a cone with a 45 degree vertex angle (directed upstream) and a cylindrical stem section of 200 mm in length and 20 mm in diameter that screwed into the sting. A schematic representation of the cone section can also be found in Figure 3.4. Two of these cone sections were fabricated with base diameters of 89.4 and 141.4 mm, representing blockage ratios of 20 and 50 percent. Each cone section was turned from a single piece of aluminum and machined with sharp edges.

A unique instrument was used to support the four hot-wires in the measuring section. This probe holding apparatus was inserted and secured in the measuring section downstream of the cone piece. It presented a total flow blockage of approximately eight percent. A schematic representation of this apparatus is shown in Figure 3.5. The probe holding apparatus was fabricated using a central bar, a nose piece, and two stabilizing pieces. The downstream stabilizing piece was secured with screws that passed through the wall of the plexiglass pipe to anchor the upper and lower sets of three angularly equidistant spokes. The hollow aluminum central bar was free to slide through the downstream stabilizing piece and could be held in the desired location by the clamping collar. The upstream stabilizing piece had three angularly equidistant spokes that butted against the pipe wall but were not secured by screws. This piece traversed with the central bar and was used to damp gross

Note: "d" can
equal 89.4 mm
or 141.4 mm.

PLEXIGLASS PIPE
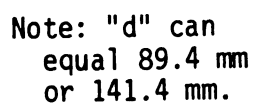
Scale : 1mm = 3.5 mm

Figure 3.4   Measuring Section with Cone.
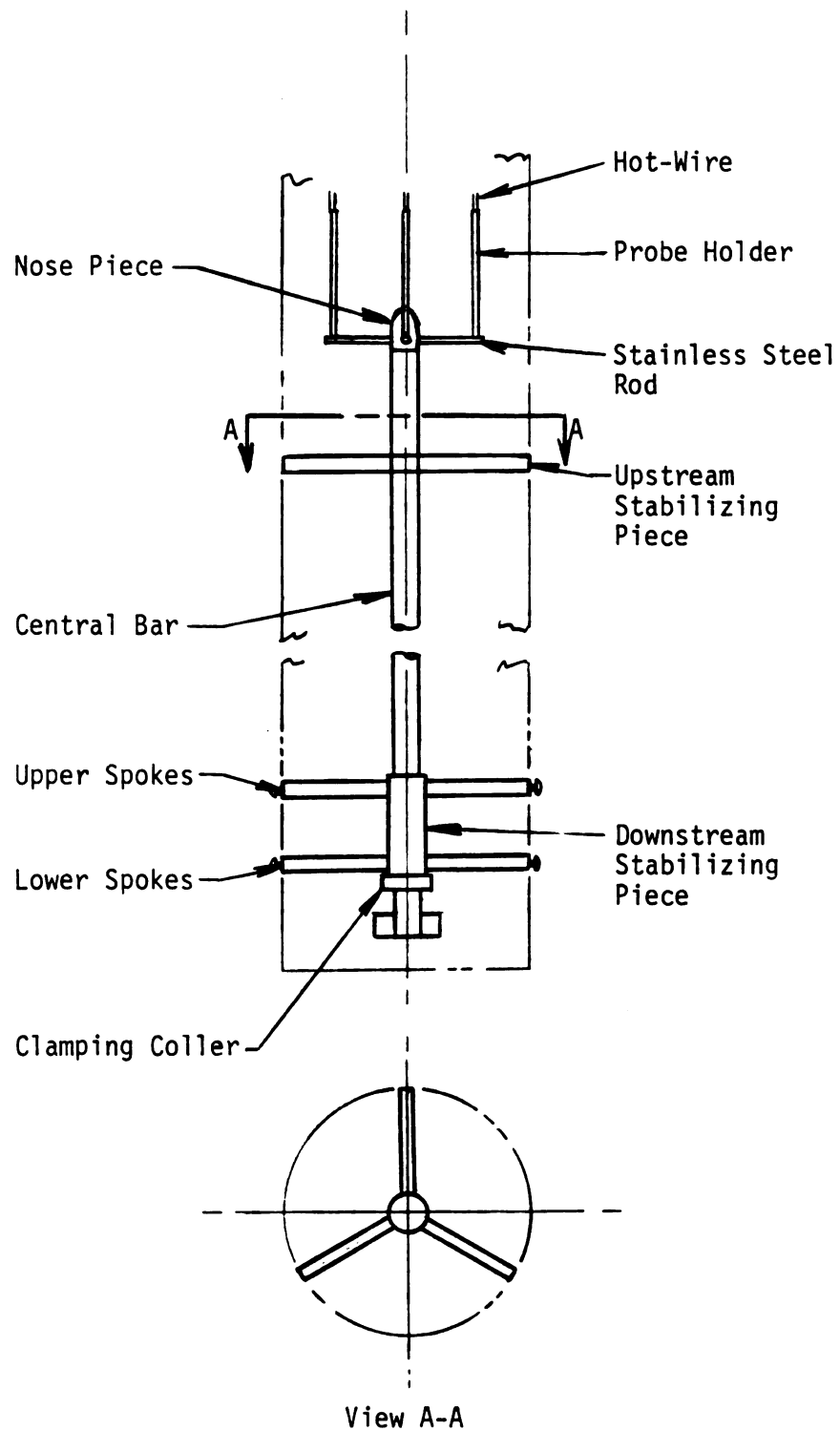
Figure 3.5 Probe Holding Apparatus.

vibrations which might have otherwise occurred due to the cantilever geometry of the probe holding apparatus. The removable PVC nose piece held four stainless steel rods in a constant axial plane at prescribed angular displacements. Each of these rods was used to hold a brass tube (which served as a probe holder) in the upstream direction. DISA hot-wire sockets fit snugly into these probe holders. Three nose pieces were fabricated, each corresponding to one of the three unique angular arrays of the four hot-wire probes. The nose piece shown in Figure 3.5 corresponds to one such array.

A variable position probe holding apparatus was used for the experiments that required only one hot-wire probe. The location of the measurement position for the spectral analysis, determined from the results of the experiments performed using this device, was used to determine the dimensions of the hot-wire probe holding apparatus of Figure 3.5. The variable position probe holding apparatus was similar in design to the apparatus of Figure 3.5 except that it had only one steel rod extending from the nose piece to support the brass probe holder, and it was capable of traversing a single hot-wire probe in the x, r, or theta directions.

The high fluid velocities that occur in the test section were found to generate vibrations in the hot-wire sockets at the ends of the 190 to 210 mm long brass tubes. A fishing line of 0.16 mm diameter was used to stabilize the brass rods. The fishing line was wrapped near the free end of the

rod and tied to the bases of the two neighboring brass probe holders. This is schematically shown in Figure 3.6.

3.2. Instrumentation

Both hot-wire and LDA measuring techniques were used for this experiment. Hot-wire measurements form the bulk of the data, while the LDA measurements were used for validation of the location of the hot-wire measurements. The hot-wire instrumentation and computer hardware are described in Subsection 3.2.1.. Subsection 3.2.2. contains information on the LDA instrumentation.

3.2.1. Hot-Wire

The instrumentation used for the hot-wire measurements consisted of hot-wire anemometers, hot-wire probes, low pass filters, an oscilloscope, and a computer. The hot-wire instrumentation is shown in Figure 3.7. The four anemometers, manufactured by Prosser, had many convenient features, one being a percentage overheat selection which automatically set the operating resistance of the hot-wire. The output voltage range for the anemometer was either 0-10 V or 0-3.33 V, depending on the chosen output port. The small output voltage range was useful for the analog-to-digital input of the computer. The hot-wire probes used in this experiment were single straight wires manufactured by DISA. A hot-wire welding apparatus allowed quick, on-location repair of the 1 mm long, 5 micron diameter, platinum-plated tungsten wire. A 10 kHz low-pass filter was

Probe Socket

Brass Probe Holder

Fishing Line

To base of nearest
brass probe holder

To base of nearest
brass probe holder

Nose Piece

Stainless Steel Rod
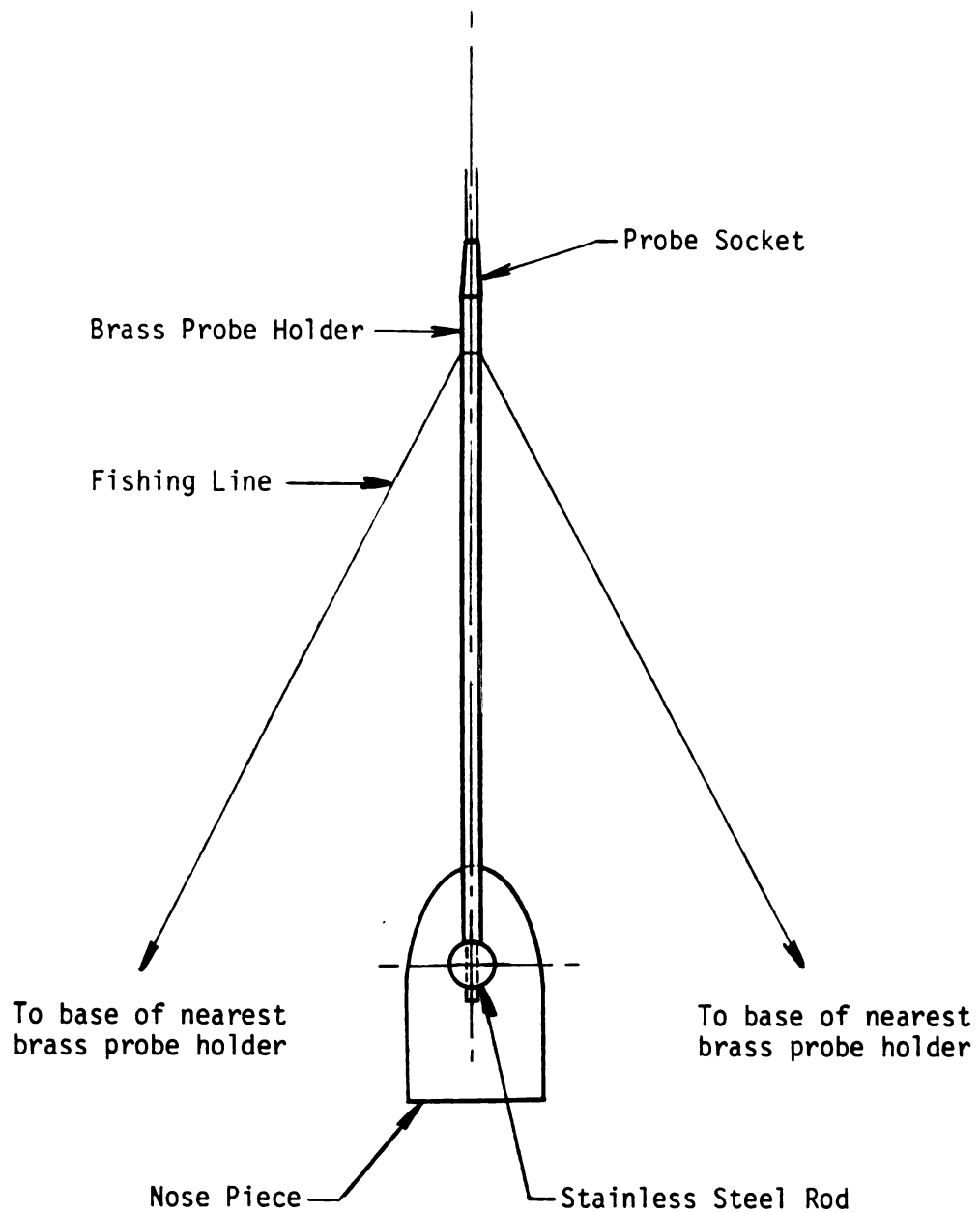
Figure 3.6 Brass Probe Holder Secured by Fishing Line.

Hot-Wire
Inputs

| Prosser   2-Channel
Hot-Wire Anemometer | | Posser   2-Channel
Hot-Wire Anemometer |

Oscilloscope

| 10 kHz
Low-Pass
Filter | 10 kHz
Low-Pass
Filter | 10 kHz
Low-Pass
Filter | 10 kHz
Low-Pass
Filter |

A/D   BOARD

Hewlett-Packard 1000
A600 Computer
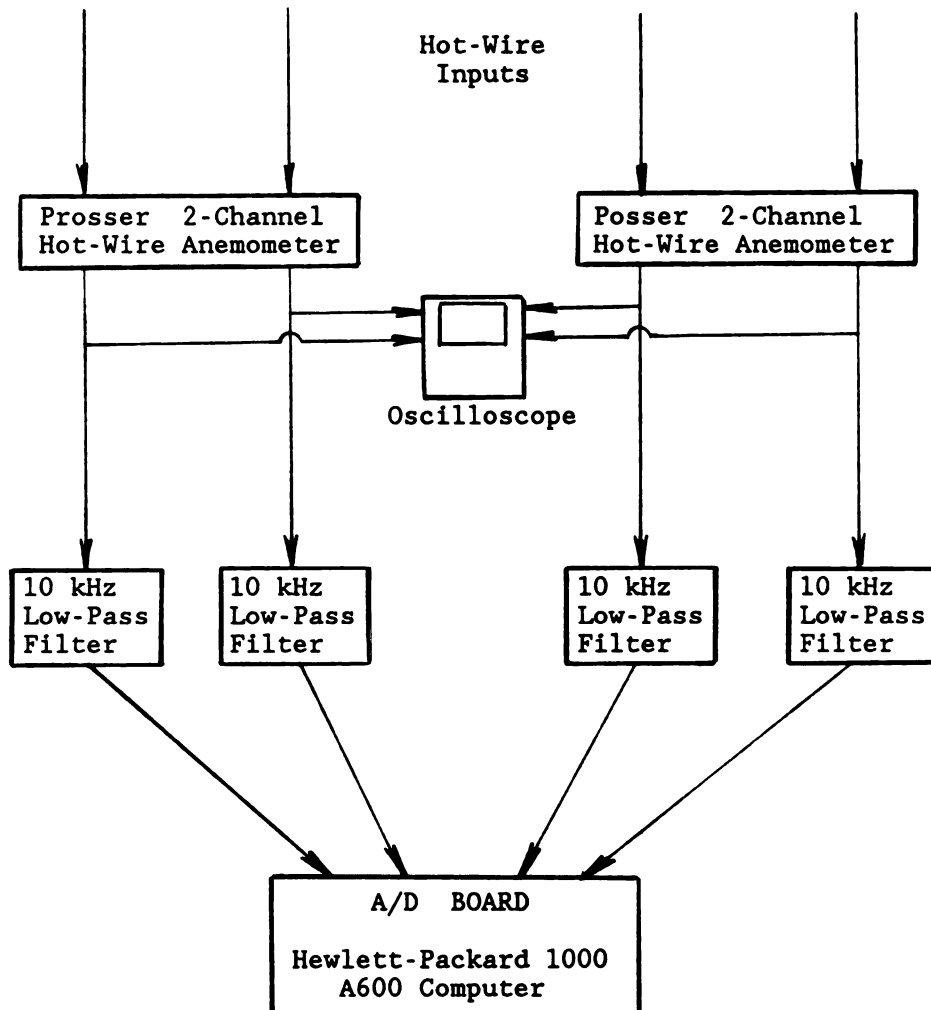
Figure 3.7   Hot-Wire Instrumentation.

used on each of the hot-wire outputs. These filters were
fabricated by the electronic shop at the LSTM.   The
oscilloscope was mainly used as a visual check on the hot-
wire signals.   It proved   invaluable for diagnosing
extraneous sources of noise.   The computer was a Hewlett
Packard 1000 A600 model.   The memory storage rate of the
computer allowed four channels of 2048 samples per channel
to be stored in one data block.   The number of blocks
written to memory depended on the amount of available hard
disk space.

3.2.2. Laser-Doppler Anemometer

The LDA system was configured in the forward scatter
arrangement. This mode yields the strongest signals for any
type of flow but it was especially desirable in the case of
this lightly seeded flow. The LDA set-up is shown in Figure
3.8. The set-up was greatly simplified by the fact that no
traversing apparatus was required, since only a one-point
single component measurement was desired.

The components of the LDA system were a laser, the
transmitting   optics,   the   receiving   optics,   a
photomultiplier, a filter, and a counter. Details of the
transmitting and receiving optics are shown in Figure 3.8.
A 15 mW helium-neon NEC laser (wavelength of 632.8
micrometers) was used in the LDA system.   The half angle
between the laser beams was 5.83 degrees. The LDA probe
volume (shaped like an ellipsoid) had approximate axis
lengths of a = 0.0405 mm, b = 0.0403 mm, and c = 0.4 mm.
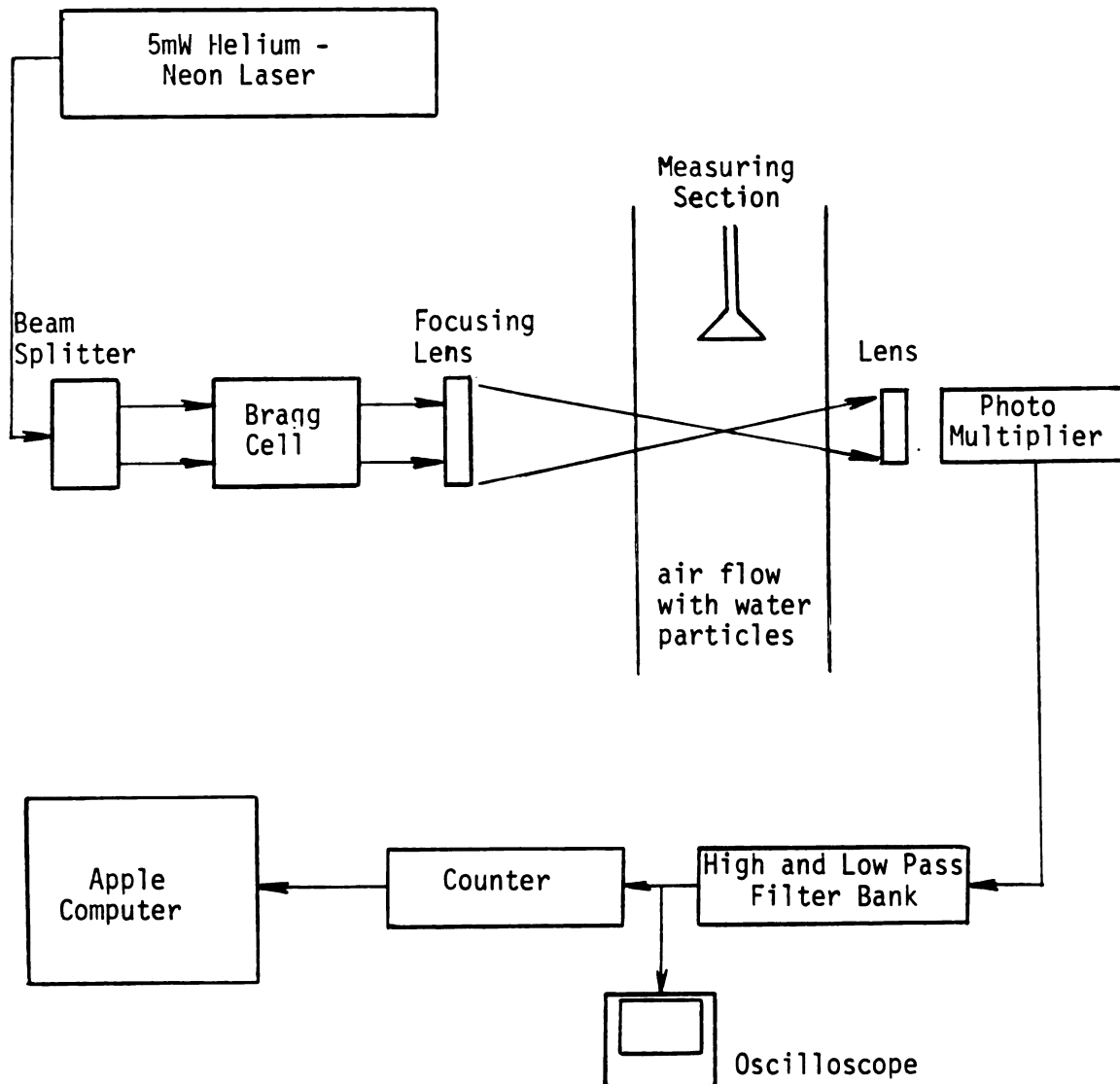
Figure 3.8   LDA Set-Up and Instrumentation.

The equations used for these calculations are from Durrani and Greated (1977). The light scattering particles were water droplets of approximately 1 micron diameter supplied by a pressure atomizer located near the contraction inlet in the upper plenum. The input signal to the counter was both high pass and low pass filtered so that it contained only the Doppler frequency with a minimum level of noise. An oscilloscope was used to view the Doppler bursts during signal optimization and data taking. The counter was fabricated at Imperial College of Science and Technology in London, England. The output of the counter was read by an Apple computer.

4. DATA ACQUISITION AND PROCESSING

A detailed description of the experimental procedure is contained in Subsection 4.1.. A summary of the computer software is presented in Subsection 4.2.. Subsection 4.1. is further divided into five subsections, each pertaining to a separate experiment. Details of the documentation of the approach flow are covered in Subsection 4.1.1.. Subsection 4.1.2. contains information on the analysis of the hot-wire signal on its route from the laboratory to the computer room. Procedures for determining the optimum hot-wire measurement position and the effect of the probe holder on the flow at that measurement position are covered in Subsections 4.1.3. and 4.1.4.. The procedure for determining the sampling frequency for the hot-wire spectral study is contained in Subsection 4.1.5. and details of those hot-wire measurements are presented in Subsection 4.1.6..

4.1. Experimental Procedure

4.1.1. Documentation of Approach Flow

The documentation of the approach flow was performed to quantify the degree of flow symmetry. Two procedures were utilized for this purpose: i) velocity profiles, and ii) surface streaking. The velocity profiles were used to document the air flow from the contraction outlet and were performed without the plexiglass pipe and cone in position. The surface streaking was performed on the cone and served as a visual check on the axisymmetric conditions. The

26

surface streaking analysis on the base of the cone also served to yield information on some details of the time-averaged shape of the recirculation region.

Two velocity profiles were measured with a single hot-wire probe at the outlet of the contraction leading to the measuring section. The velocity profiles were generated in perpendicular planes and spanned the diameter of the contraction outlet with measurements at 10 mm intervals. The location of the velocity profiles are shown in Figure 4.1.

The surface streaking was performed in the measuring section with a mixture of lamp black and kerosene applied on the 50% blockage cone. The surface streaking mixture was applied over the top, base and stem of the cone and allowed to dry in the approach flow. The results were documented with photographs. The surface streaking procedure was performed on two separate occasions. The results from the first set of data suggested that the flow around the cone was not axisymmetric. This lack of axisymmetry was assumed to be caused by sporadic and small amplitude vibrations of the cone (only the 50% blockage cone showed these vibrations). To stabilize the 50% blockage cone, piano wire of 0.15 mm was looped around the stem, passed through the joint of the measuring section and contraction, and anchored by screws that provided adjustable tension. The flow disturbance caused by the piano wire ceased well before the top of the cone was reached. The calculations that support this assertion can be found in Appendix A. Only the 50%
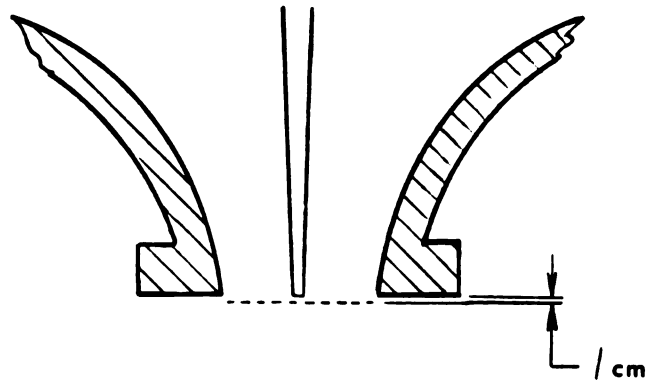
Location of velocity
profiles represented
by dotted lines
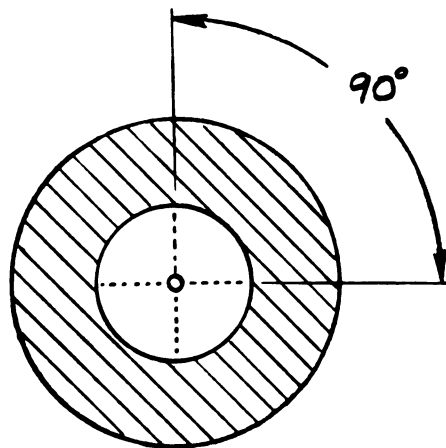
Figure 4.1 Velocity Profile Locations at Contraction
Outlet.

blockage cone was stabilized. A drawing of the stabilized cone is shown in Figure 4.2. The surface streaking procedure was then performed a second time to verify the axisymmetry of the flow around the cone.

4.1.2. Documentation of Hot-Wire Signal

The hot-wire signals were routed from the laboratory to the computer room where they were digitized and stored on a computer disk. Two different types of checks were performed to determine sources of noise. One check used a hot-wire signal and an oscilloscope, and the other used a DC power supply and a voltmeter. In both cases the electrical signal was routed along the same path used for the hot-wire signal transfer to the computer. This path is shown in Figure 4.3. One source of noise (discovered while using the hot-wire and oscilloscope) was removed by installing a constant voltage transformer between the power outlet and the hot-wire anemometer. A high frequency noise signal (approximately 50 kHz) was removed by passing the hot-wire signal through a 10 kHz low pass filter.

The voltage check using the DC power source was used to identify any attenuation of the signal. The power source was connected to all four channels in the laboratory and the voltages were checked before entering the low pass filter and after exiting the filter and A/D board. As expected, there was no discernable change in the voltages before and after the low pass filters.

The spectral analysis portion of the investigation
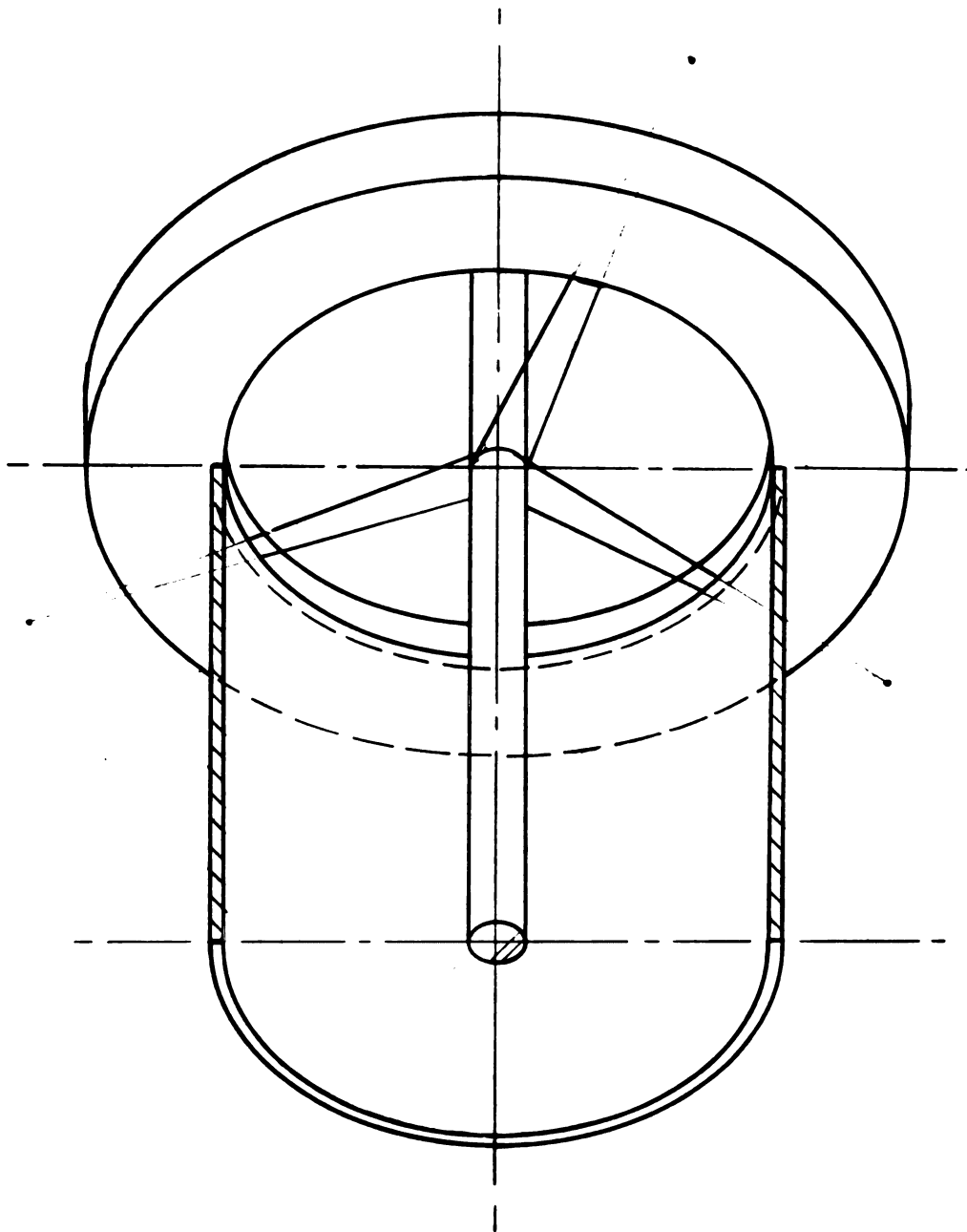
Figure 4.2 Stabilized 50% Blockage Cone (neck section).
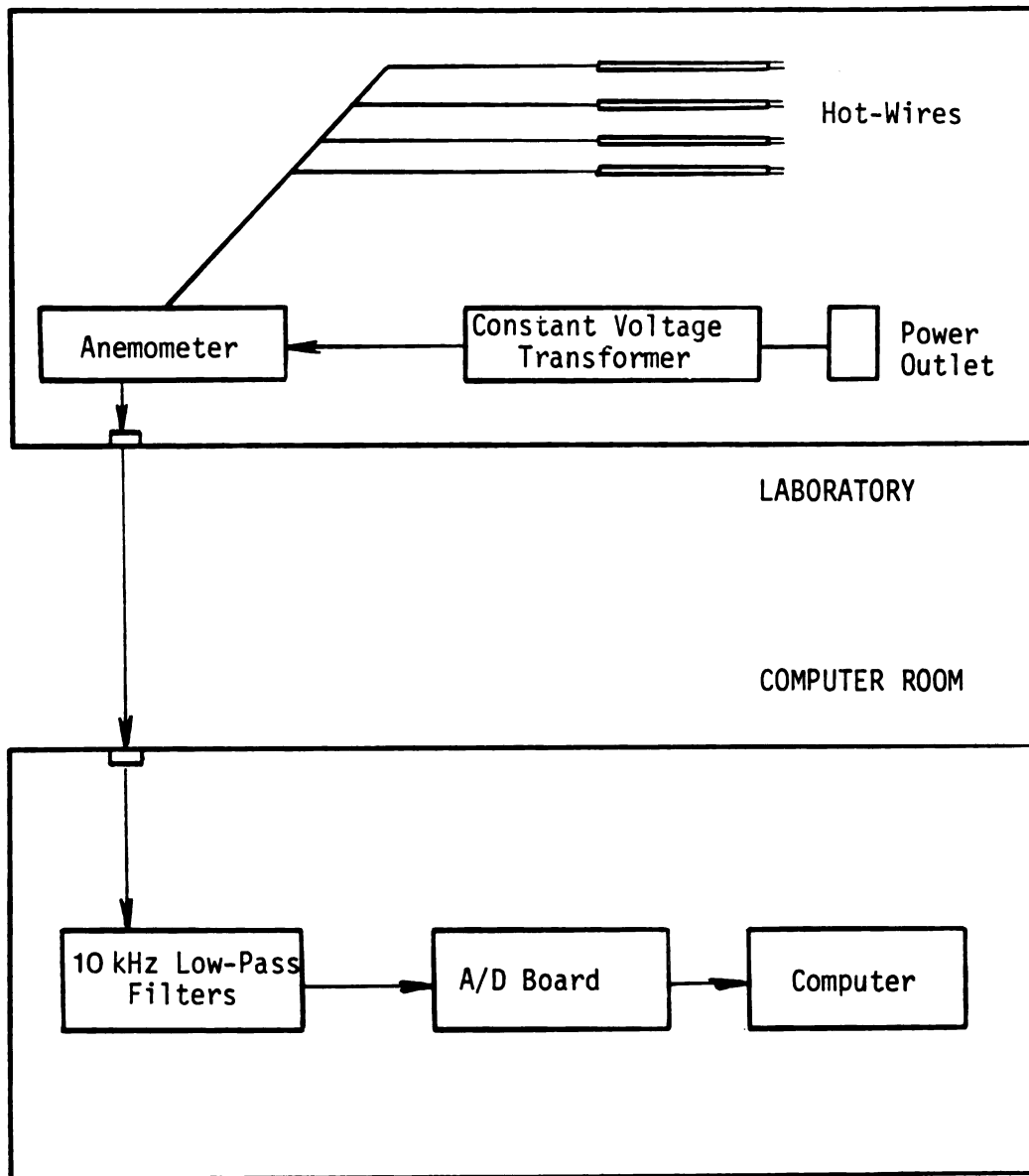
Figure 4.3 Hot-Wire Signal Path.

required the simultaneous sampling of four hot-wire probes to yield information on any large-scale motions of the turbulence. Any difference in phase shifts introduced by the low pass filter would be undesirable. A phase check of signals before and after low pass filtering was performed using a high frequency sine wave. A 5 kHz sine wave was introduced simultaneously into the four low pass filters and the outputs were checked against one another on an oscilloscope. The four filters were found to introduce an identical phase shift of 80 degrees into each sine wave; hence, there was no need for further phase matching of the filtered hot-wire signals.

4.1.3. Determination of Measurement Locations for the Spectral Analysis

The optimal measurement location that would enable detection of coherent motions in this flow geometry would be in the irrotational flow between the wall boundary layer and the widest point of the circulation region aft of the cone. Three experiments were performed to define a measurement location for the hot-wire probes. These three experiments were also performed to yield information on the recirculation region. The first experiment located the wake or vortical fluid generated near the separation stream surface of the cone recirculation region. This was followed by an experiment in which wall tap pressure profiles were recorded over a length of the cone recirculation region. Finally, tentative measurement positions for both cones were

chosen, and velocity and velocity root-mean-square (rms) profiles were obtained at these locations.

The experiment detecting the wake boundary was performed in the measuring section with the cone in place. The anemometer output from a single straight hot-wire mounted on a traversing probe holder was used in conjunction with an oscilloscope to visually determine areas of vortical and irrotational fluid. The starting position of the hot-wire was in the axial plane containing the base of the cone approximately 1 mm from the edge of the base. The hot wire probe was traversed in the positive axial (x) direction to document the spread of the wake. At each axial location the probe was traversed back and forth radially to determine a time averaged location for the boundary defined by 50% intermittancy of vortical fluid at the measurement locations. This was continued through positively increasing axial locations until the wake was not discernable from boundary layer of the wall or until the end of the probe traverse was reached.

The pressure profiles were recorded through the use of wall taps in the plexiglass pipe of the measuring section with the cone in place. The wall taps were positioned lengthwise along the pipe, but they did not extend to the tail of the recirculation region generated by the cone. Two separate pressure profiles were taken since the 50% blockage cone extended farther down into the measuring section than the 20% blockage cone.

Using information from the two studies mentioned above,

measurement locations for the cone study were chosen for the two blockage ratios. In both cases the measurement location was selected as a compromise between, i) being as near as possible to the wake of the cone while staying in the irrotational fluid and, ii) being as near as possible to the axial plane containing the widest point of the recirculation region (the wake eventually spread across the entire diameter of the pipe before this location was reached).

Velocity and velocity rms profiles were taken using a single straight hot-wire probe traversed in the axial direction through the same radial position as the measurement location. The velocity profile served as an aid in determining the shape of the time-averaged recirculation region. The velocity rms profile gave a measure of the flow's unsteadiness.

4.1.4. Determination of Effect of Probe Holder

Two studies were performed to determine if the presence of the probe holder changed the flow at the proposed hot-wire measurement location for the spectral analysis. These two studies were conducted only for the case of the 50% blockage cone. Because the nose of the probe holding apparatus extended up to $x/d=1.9$ for the 50% blockage cone and only up to $x/d=3.0$ for the 20% blockage cone, it was assumed that the results of the studies on the 50% blockage case (the most stringent case) could be applied to the 20% blockage case. The first study entailed performing wall tap pressure

profiles with and without the probe holder in the measuring section. This was followed by a second study in which a one-point LDA measurement was taken near the approximated close of the recirculation region with and without the probe holder in the measuring section.

The pressure profile study was conducted using the wall taps in the plexiglass pipe of the measuring section. Initially, the pressures were read from the wall taps with the probe holding apparatus installed in the measuring section. The probe holding apparatus was then removed from the measuring section without turning off the flow system and the pressures were read again. The pressure difference between the wall tap and plenum was non-dimensionalized using equation 2.1.

The LDA system was set up in a forward-scatter mode to take a series of one-component measurements at a single location. The location of the measurements was along the central axis of symmetry of the pipe section at an axial location of x/d=1.3. Taylor and Whitelaw (1984) found the length of the recirculation region aft of a cone of 25% blockage ratio and 45 degree vertex angle to be 1.55 cone diameters. Winterfeld (1965) found the length to be 1.7 cone diameters for a similar cone of 25% blockage. Since a 50 percent blockage cone would be expected to have a longer recirculation region than that of a 25% blockage cone, (a trend observed by Taylor and Whitelaw (1984) for disks), the axial location of x/d = 1.3 for the present LDA measurement was inferred to be within the recirculation region aft of

the 50% blockage cone.   This location was targeted as an area that would be sensitive to the introduction of a downstream flow obstruction and thus show the effects, if any, of the probe holding apparatus. Because the LDA measurement location was in an area where the direction of the flow was unknown, two Bragg cells were used to add a 3 MHz frequency shift to one of the laser beams. The filtered photomultiplier output yielded Dopler frequencies that were processed by a counter.   Velocity and velocity rms values were taken with and without the probe holding apparatus in position.

4.1.5. Determination of Sampling Frequency for the Spectral
         Analysis

  The sampling frequency of the hot-wires for the spectral analysis was established using three guidelines. They were defined as, i) to sample fast enough to ensure adequate representation of the power spectrum, ii) to have sufficient samples in a contiguous data block to contain information on a motion occurring on the integral length scale (large scale motion) and, iii) to have sufficient samples in a contiguous data block to contain information that represented enough motions occurring on the integral length scale to provide reliable statistics. An evaluation of the first criterion entailed creating power spectra plots from the information from a single hot-wire located in the irrotational flow at the measurement location (defined in Subsection 4.1.3.) for the 50% blockage cone and determining

the smallest acceptable sampling frequency. The first test
was an averaged power spectrum, defined as the square of the
velocity rms as a function of frequency, created from ten
statistically independent blocks of data (containing 1024
data points per block) sampled at a frequency of 2000 Hz.
Two plots of this averaged power spectrum, one on a
logarithmic scale, are shown in Figure 4.4. The plots of
Figure 4.4 suggested very few flow disturbances occurring
at frequencies of 400 Hz and above. Thus, the sampling
frequency for the cone study was chosen as 800 Hz; this
allows frequency resolution up to 400 Hz.

The second criterion dealt with the amount of contiguous
data points that could be stored on the available data
acquisition system. The following analysis was performed to
ensure that the number of samples in the data block were
sufficient to represent information on a motion occurring on
the integral length scale.

The integral length scale, l_i, for this geometry was
selected as the cone diameter, d:

$$l_i \cong d, \tag{4.1}$$

where d = 141 mm for the 50% blockage cone and 89 mm for the
20% blockage cone. With an approach flow velocity of

$$U_o = 12.2 \text{ m/s},$$

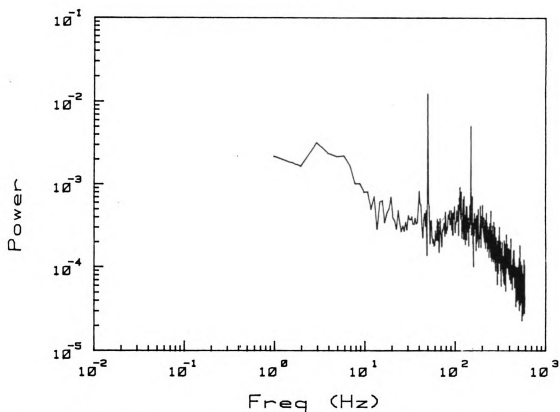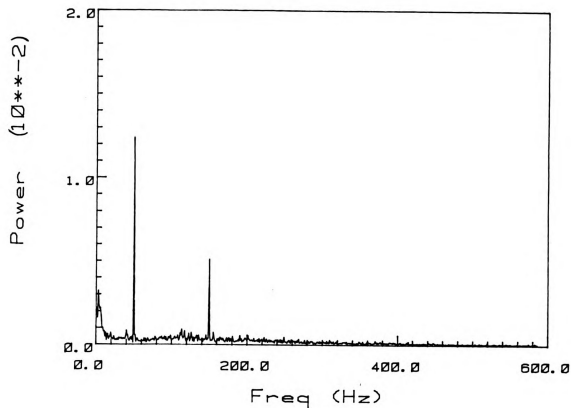estimates of the maximum and minimum convection velocities

Figure 4.4 Average Power Spectra of Hot-Wire Data at Measurement Location Shown on Two Scales.

occurring in the irrotational flow around the wake region
are

$$U_{max} \cong 20 \text{ m/s}$$

$$U_{min} \cong 5 \text{ m/s.}$$

The estimate for the maximum convection velocity arose from
the axial velocity profile (half the largest observed
velocity) and the estimate for the minimum flow speed was
taken as slightly less than half the approach flow velocity.
The time required for the passing of one convective length,
for the most conservative case (in terms of largest amount
of data storage space), would be

$$t_c = l_i/U_{min} = 0.141/5 = 0.028 \text{ sec.} \qquad (4.2)$$

The following number of samples required for information on
a single motion occurring on the integral length scale is
calculated by multiplying the time required for the passing
of one convective length by the sampling frequency:

$$s = (t_c)(800 \text{ Hz}) = 23 \text{ samples.} \qquad (4.3)$$

Therefore, a block of contiguous data containing 2048
samples enables representation of information on 89 such
motions of the integral length scale.

The third criterion dealt with the total number of large

scale motions represented by the data. Ten independent blocks of data containing 2048 samples per block were stored. Since one data block was capable of representing nominally 89 large-scale motions, ten blocks allowed representation of 890 of these motions.

4.1.6. Hot-Wire Measurements for the Spectral Analysis

The configuration of the hot-wires for the gathering of the time series information for the spectral analysis consisted of three arrays of four single, straight hot-wire probes. The four hot-wires in each array were positioned at the axial (x) and radial (r) measurement locations described in Subsecton 4.1.3., but each array had differing angular displacements between the individual probes. The configuration of the three arrays are depicted in Figure 4.5.

The entire measurement procedure was completed for the 50% blockage cone and then repeated for the 20% blockage cone. For each of the three arrays, the four hot-wires were simultaneously sampled at a rate of 800 Hz per wire. The time series were stored in ten binary data blocks with 2048 contiguous data points per hot-wire per block. The Reynolds number (based on the measuring section diameter) of the approach flow was 2.0×10^5.

The calibration of the hot-wires was performed inside the measuring section. The cone obstructed the upward traverse of the probe holding apparatus used for the spectral analysis experiment. Therefore, the hot-wires were
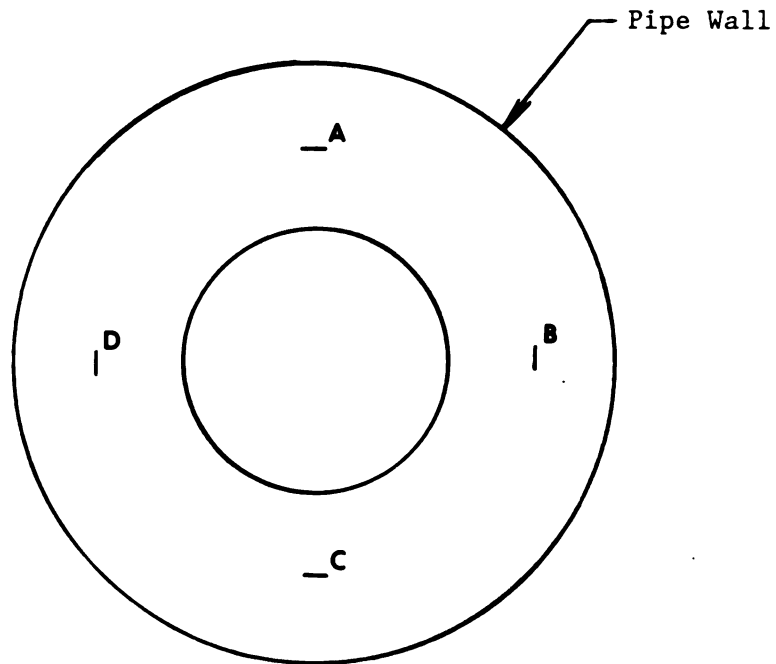
θ_i = clockwise angular displacement between
hot-wire A and hot-wire i (i = B,C,D)

Array 1: $\Delta\theta_B$ = 90°
          $\Delta\theta_C$ = 180°
          $\Delta\theta_D$ = 270°

Array 2: $\Delta\theta_B$ = 30°
          $\Delta\theta_C$ = 60°
          $\Delta\theta_D$ = 240°

Array 3: $\Delta\theta_B$ = 19° ⎫
          $\Delta\theta_C$ = 186° ⎬ ——— random displacement
          $\Delta\theta_D$ = 248° ⎭

Figure 4.5 Hot-Wire Configuration for the Three Arrays.

calibrated near the mid-section of the cone, see Figure 4.6. The velocity at this location was slightly greater than the known value of the approach flow velocity which resulted in an erroneous calibration of the four wires. Although a correct calibration of the hot-wires was desired, it was not considered necessary since the anticipated data processing (Fuchs et al (1979) technique) was of a comparative nature, e.g., auto-correlations and cross-correlations. Note that all the other experiments performed with hot-wires had correct calibrations.

4.2. Data Processing

The data sampling and processing software consisted of six programs, a sampling routine, a data transforming routine, cross- and auto-spectrum routines, an averaging routine, and a hot-wire calibration routine. The data sampling routine, the auto- and cross-spectrum subroutines and the hot-wire calibration routine were coded by Dr. Cameron Tropea of the LSTM. The data sampling routine, a general purpose measurement program for analog signal analysis, was used for the spectral analysis study. Some of the options were the selection of the number of A/D channels to be sampled (one to four), sampling frequency, number of samples per channel, and number of data storage blocks. The data points were stored in binary form. The data transforming routine read binary data files and stored each block of data in separate files in ASCII form. The averaging routine created a single data file from the average of a user specified number of
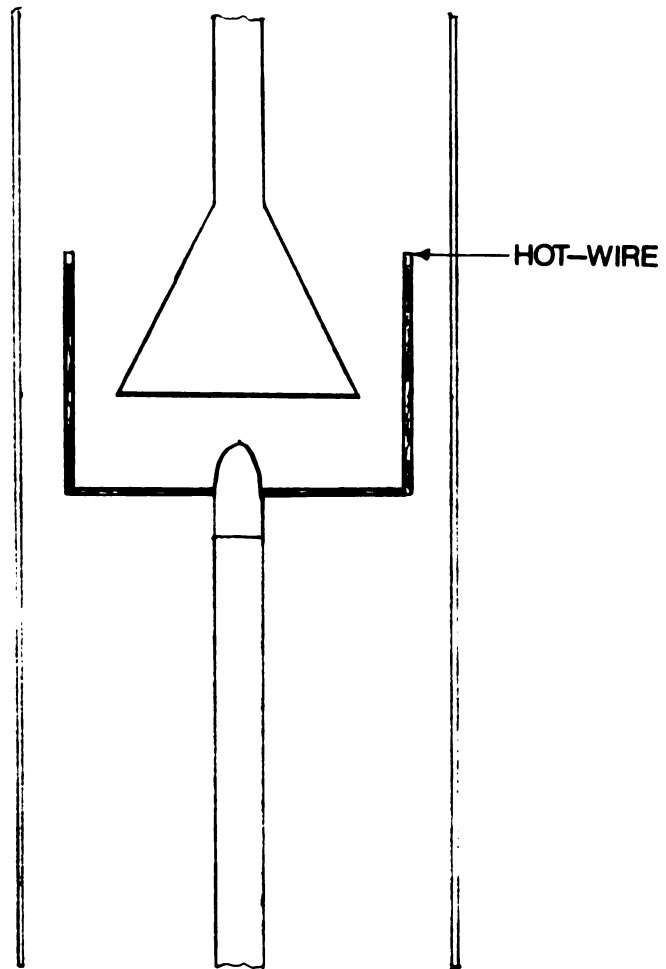
HOT—WIRE

Figure 4.6 Calibration Location for Hot-Wire in Spectral
Analysis Study.

input data files. The hot-wire calibration routine simultaneously calibrated up to four hot-wire probes. It used anemometer and pressure transducer signals and a least squares fit to determine the constants in the equation

$$E^2 = A + BU^n \qquad (4.4)$$

where E is the voltage and U is the velocity.

5. RESULTS AND DISCUSSION

The results and interpretation of the various studies outlined in the previous section are presented in the following four subsections. The velocity profiles and surface streaking pictures of the flow symmetry check are presented in Subsection 5.1.. The results associated with the studies performed for the determination of the measurement location are found in Subsection 5.2.. Subsection 5.3. contains results from the study on the flow effects of the probe holding apparatus. Subsection 5.4. contains the results from the spectral analysis.

5.1. Results of Experiments Performed
for Flow Symmetry Check

The symmetry of the fluid flow around the conical obstruction was analysed using surface streaking and a series of velocity profiles. A velocity profile taken 10 mm downstream of the contraction outlet (without cone and measuring section) is presented in Figure 5.1. Figure 5.2 presents the velocity profile taken at the same downstream locations but in a direction that is perpendicular to the first traverse. The troughs located at the center and edges of the plot (on the axis labeled "outlet diameter") correspond to the velocity deceleration introduced by the centered sting and the edges of the contraction. The positioning of the hot-wire probe traverse in preparation for the measurements was done by eye and has an associated error of approximately plus or minus 3.0 mm.
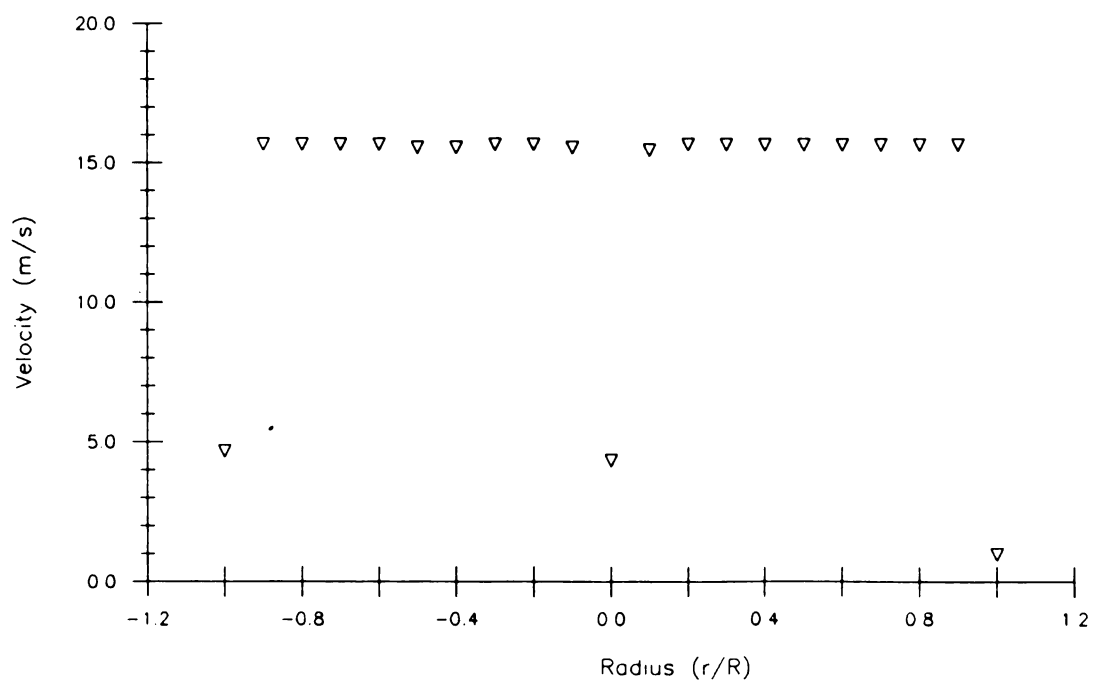
**Figure 5.1 Velocity Profile at Contraction Outlet.**
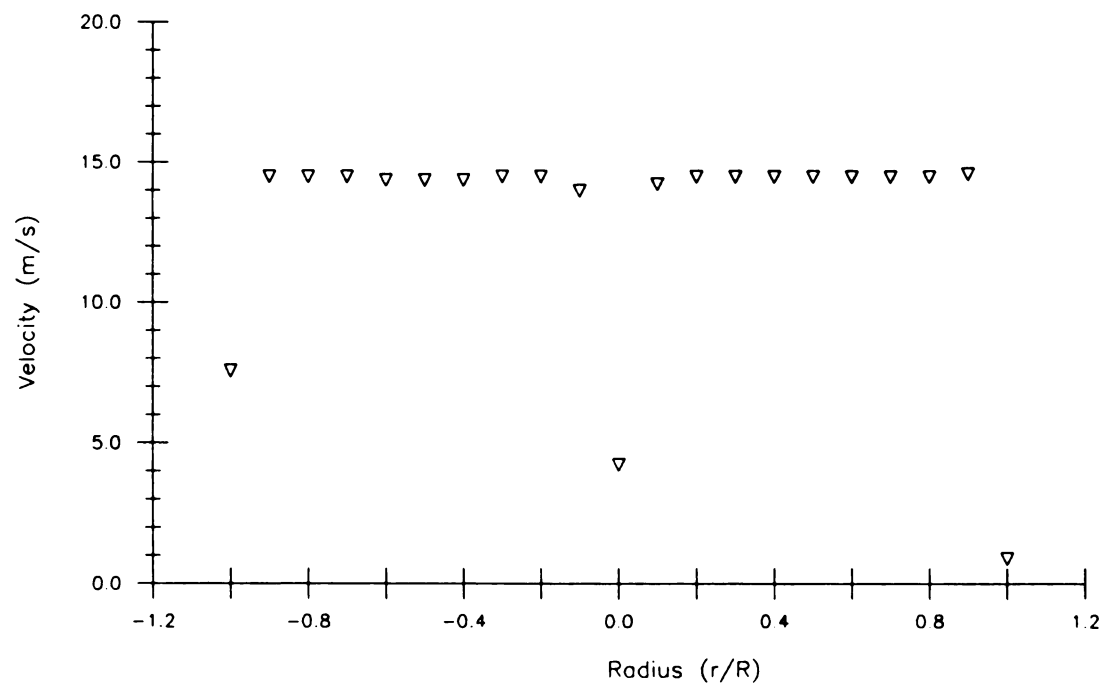
Figure 5.2 Velocity Profile at Contraction Outlet in Perpendicular Plane.

The plots of Figures 5.1 and 5.2 suggest that the flow exiting from the contraction is axisymmetric. The plots show good symmetry about $r/R = 0$ within the error bounds mentioned above. For the bulk flow (omitting velocity values at the extreme edge and the sting locations), the percentage difference in velocity between the corresponding radial locations 180 degrees apart ranges from 0.7% to 0.9%. The difference in the velocity values at the nominal positions, $r/R = 1$, are associated with the positioning uncertainty and the very steep velocity gradients at these r values. The two velocity profiles were taken at separate times thus attributing to the difference in the mean velocity values of the bulk flow between the two profiles.

The results of the two surface streaking studies are presented in photographic form. The underside of the cone was the only area where effects of the use of piano wire for stability could be readily observed. Figure 5.3 presents photographs of the base of the 50% blockage cone before and after the addition of the piano wire. Photograph A clearly shows an accumulation of the lampblack fluid toward one area near the edge of the underside of the cone. In the central region however, the brushstrokes are still visible signifying very weak shear stresses in this area. In contrast, Photograph B shows an even distribution of the lampblack fluid in a ring with a diameter slightly smaller than the base diameter of the cone. This photograph also shows a pattern of streaks radiating from the center of the cone underside, suggesting a condition of symmetry. Other
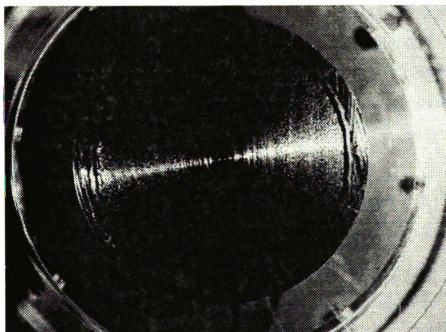
Before
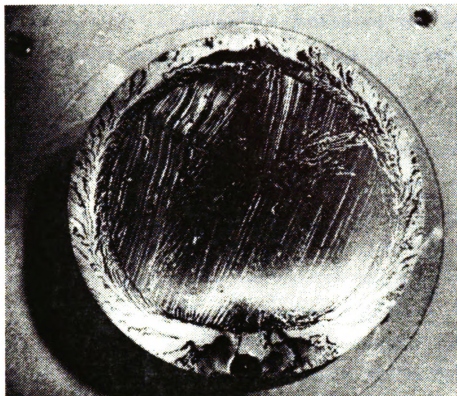
After

Figure 5.3 Surface Streaking on the Underside of the 50%
           Blockage Cone Before and After Stabilization.

notable features suggested by the lampblack fluid markings in both cases were, i) a separation bubble on the stem where the cone contour started and, ii) evenly distributed streaks running the length of the cone.

A topological evaluation of the surface streaking results shown in Photograph B of Figure 5.3 presents a convincing argument for an axisymmetric time-mean flow. The basic concepts of the following topological evaluation were provided by Foss (1988). An interior-plane surface, as defined by Foss, is appropriately represented for this flow geometry as a sphere with three holes; see Figure 5.4. To visualize this "surface", one can envision an inverted pair of trousers that has been flattened. Note that the velocity vectors are perpendicular to the exposed openings at the leg and waist (flattened) holes. Singular points are represented by areas on the surface where the continuous velocity vector field vanishes. These singular points are labeled, as defined by Hunt, Abell, Peterka, and Woo (1978), as a saddle (intersection of oppositely directed vector lines) or as a node (intersection of an infinite number of vector lines).

The interior-plane surface of Figure 5.4, which is the equivalent of a sphere with three holes, has an Euler characteristic equal to negative one. A topological theorem states that the sum of the nodes minus the sum of the saddles is equal to the Euler characteristic of the surface or, for an interior-plane surface
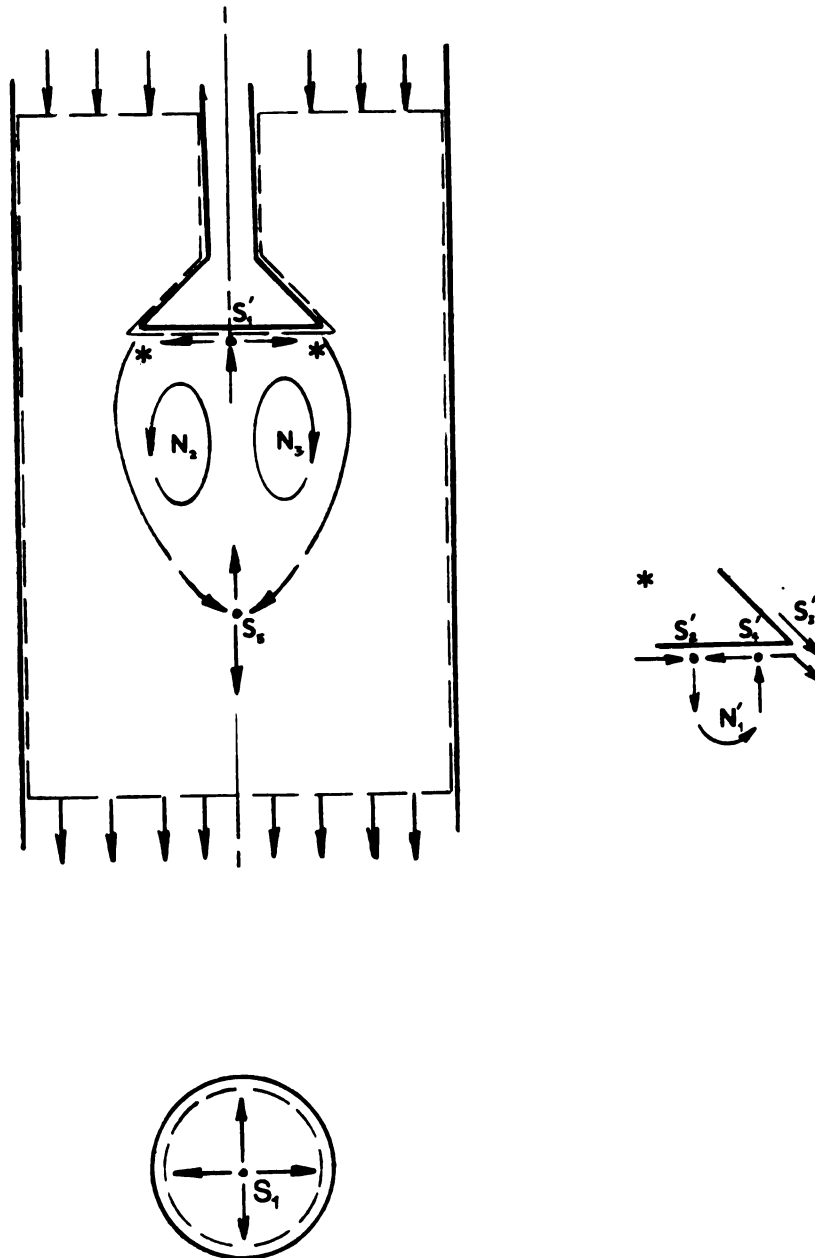
Figure 5.4 Singular Point Distribution for an Interior Plane Surface as Suggested by an Evaluation of the Surface Streaking Photograph.

$$X_{surface} = 2 \sum N + \sum N' - 2 \sum S - \sum S' \qquad (5.1)$$

where the prime indicates a "half saddle" or a "half node"; these singular points occur at the boundary of the surface. For the surface in Figure 5.4 the equation becomes

$$X_{surface} = 2 \sum N + \sum N' - 2 \sum S - \sum S' = -1. \qquad (5.2)$$

The following singular point distribution arises from the lampblack pattern on the base of the cone section. The visual markings provided by the surface streaking evaluation are depicted by velocity vectors in Figure 5.4. The radial spread of the lampblack fluid is represented by S_1'. Another half saddle, S_2', represents the ring of accumulated lampblack fluid. A half saddle, S_3', is formed at the edge of the cone where the fluid swept from the base joins the fluid flowing downstream from the side. To connect these two half saddles, there must be a half node or half saddle between them created by the velocity vectors (in opposing directions) of the supplied fluid flow. The combination of S_4' and N_1' satisfy the flow field as well as the previous equation.

The following is a description of a probable singular point distribution. A free stagnation point is assumed to exist at the tail of the recirculation region in the axisymmetric time-averaged flow. This free stagnation point

is represented by a saddle, S_5, for the diametral interior-plane. The time-averaged motion downstream of the cone's base can be represented as a toroidal vortex. This motion is represented by the two nodes N_2 and N_3. This is the simplest singular point distribution that satisfies the theorem of equation 5.1 for this interior-plane surface. The fewest number of singular points were used to describe the surface streaking results while providing a description that is compatible with equation 5.1:

$$X_{surface} = 2(2) + (1) - 2(1) - (4) \qquad (5.3)$$
$$= -1.$$

This singular point distribution is representative of an axisymmetric flow situation. A physical explanation for this singular point distribution is suggested by Foss. The separation ring is a creature of the strongly sheared base fluid that is swept aft by the through flow and the consequent effect of deceleration that this has on the radial flow from the central stagnation point on the base of the cone section. The reattaching flow past the separation ring would approach the cone's base with a relatively small velocity magnitude. Therefore, the absence of a visual record of this reattachment ring does not contradict the assumed velocity field in this topological evaluation. It is noted that a strongly diverging flow, from the separation ring to the fluid's path along the inside of the separation stream surface, is implied by this flow model.

5.2. Results of Experiments Performed for Determination of Measurement Location for the Spectral Analysis

The measurement location for the spectral analysis was chosen at $r/d = 0.65$ and $x/d = 0.4$ for the 50% blockage cone, and $r/d = 0.8$ and $x/d = 0.67$ for the 20% blockage cone. An unforseen consequence of the choice of these measurement locations is that there is only a 5.6% difference between their downstream positions from the edge of the cones (i.e., $0.4 \times d_{50} \sim 0.67 \times d_{20}$). The time-averaged location of the boundary between the annular irrotational fluid and the wake for the 50% and 20% blockage cones are presented in Figures 5.5 and 5.6, respectively. The measurement locations for the spectral analyses are denoted by crosses on the graphs. The initial positioning of the variable position hot-wire probe holding apparatus was performed manually. There is an associated error of approximately plus or minus 1.0 mm in this positioning. The radial positioning of the probe was regulated by a threaded rod and the axial positioning by hashmarks on the main body of the apparatus. The associated positioning errors are plus or minus 0.5 mm and plus or minus 1.0 mm, respectively.

The wake, as seen in the plots of Figure 5.5 and Figure 5.6, initially follows the growth of the separation stream surface. As x/d increases, the sheared fluid eventually spans the entire pipe diameter. In Figure 5.6, the emergence of the wall shear layer is seen at the largest axial location. Regions where the fluid was always irrotational were increasingly difficult to find as the hot-
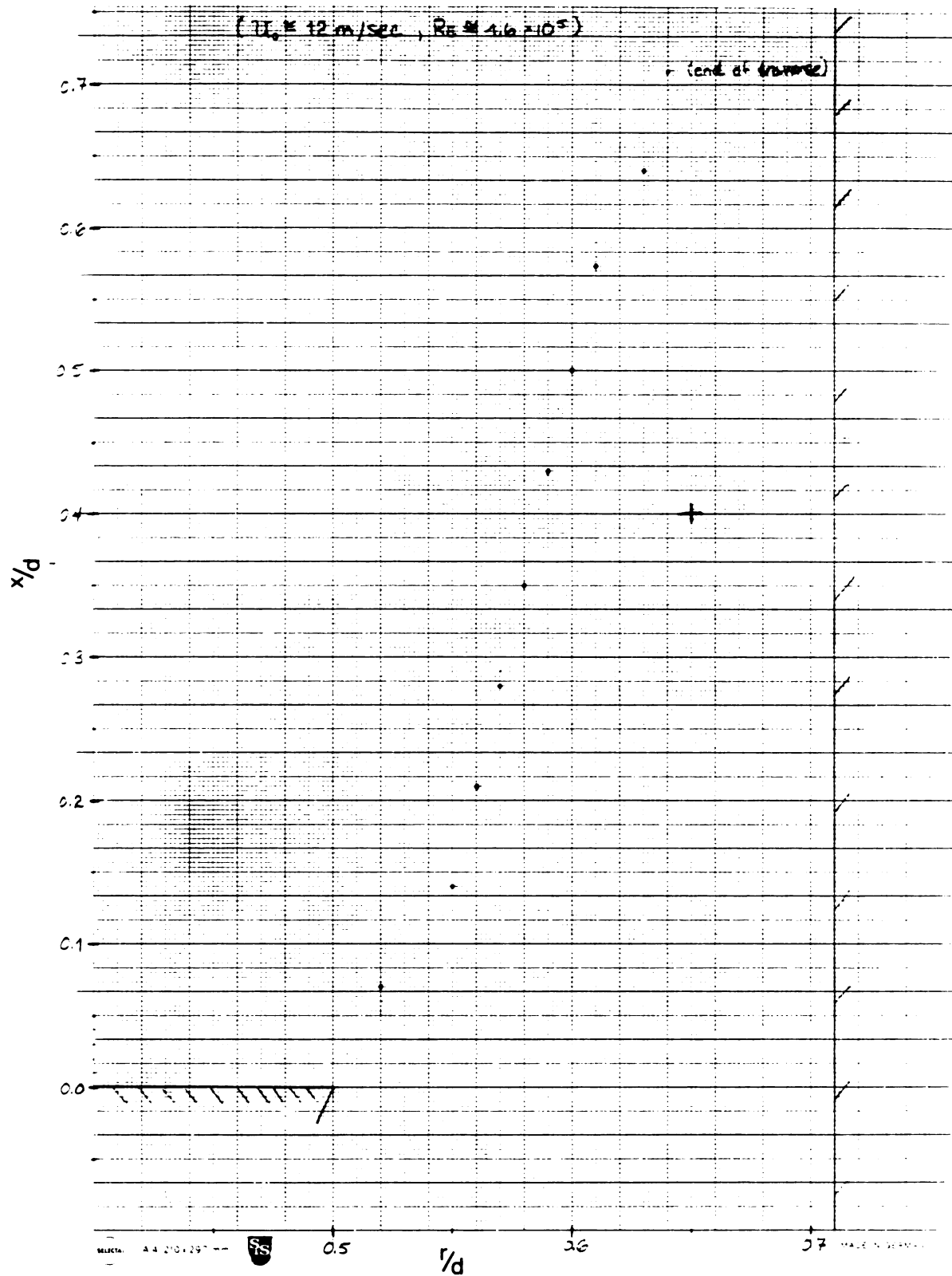
Figure 5.5 Time-Averaged Boundary Between Rotational and
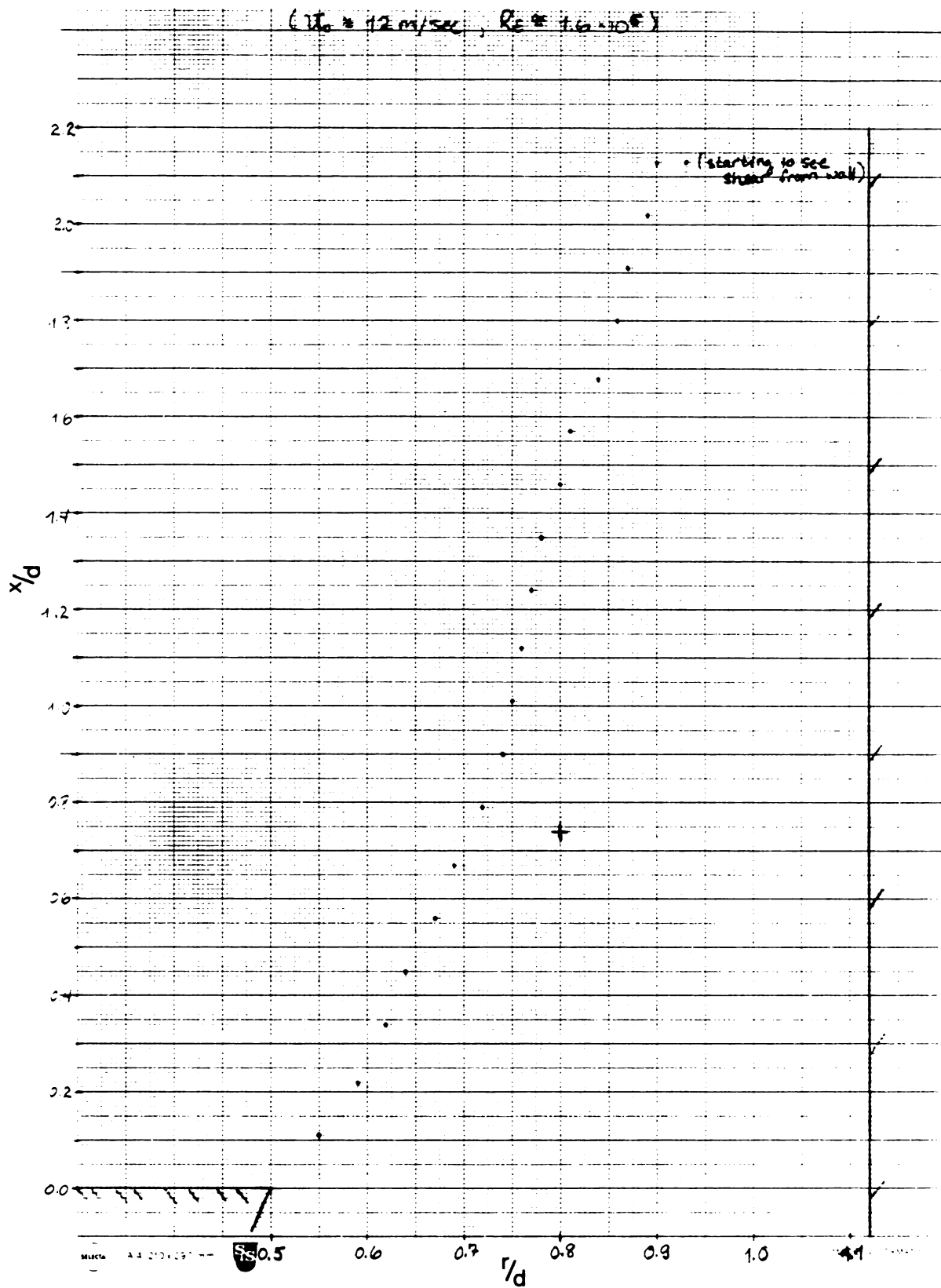Irrotational Fluid (50% Blockage).

Figure 5.6 Time-Averaged Boundary Between Rotational and
Irrotational Fluid (20% Blockage).

wire was traversed downstream. The region where the fluid flow is always irrotational is limited to approximately 1.4 cone diameters downstream of the base of the 20% blockage cone section and 0.6 cone diameters downstream for the 50% blockage cone. The approximate axial locations, where there is a 30% intermittancy of the irrotational fluid, are noted on the plots of Figures 5.5 and 5.6.

The non-dimensional static pressure profiles for the 50% and 20% blockage cones are presented in Figure 5.7. The axial position of the measurement location for the spectral analysis is represented on both graphs by a cross. The estimated error associated with the pressure measurements is plus or minus 0.5 Pa which translates to 0.005 non-dimensional pressure units. The Reynolds number (based on the diameter of the measuring section) of the approach flow was set at 1.7×10^5 with the probe holding apparatus in the measuring section. The Reynolds number of the approach flow increased to 1.8×10^5 when the probe holding apparatus was removed. It is inferred that the non-dimensional variables will be minimally effected by this small (approximately 5%) change in the Reynolds number.

The pressure profiles of Figure 5.7 serve to provide information on the shape of the recirculation region aft of the cone (see discussion in Section 2.2.). The maximum value of the pressure coefficient occurs at an axial location of x/d = 0.66 for the 20% blockage cone and at x/d = 0.78 for the 50% blockage cone. The non-dimensional axial location of the pressure minimum increases for increasing
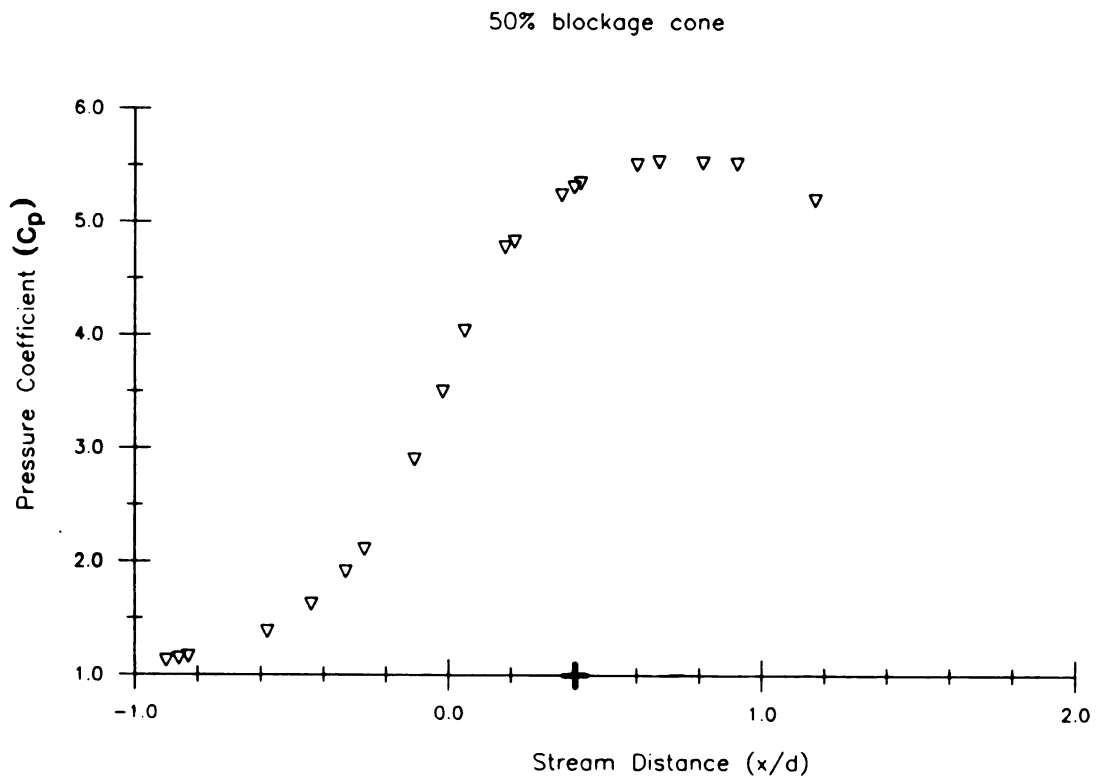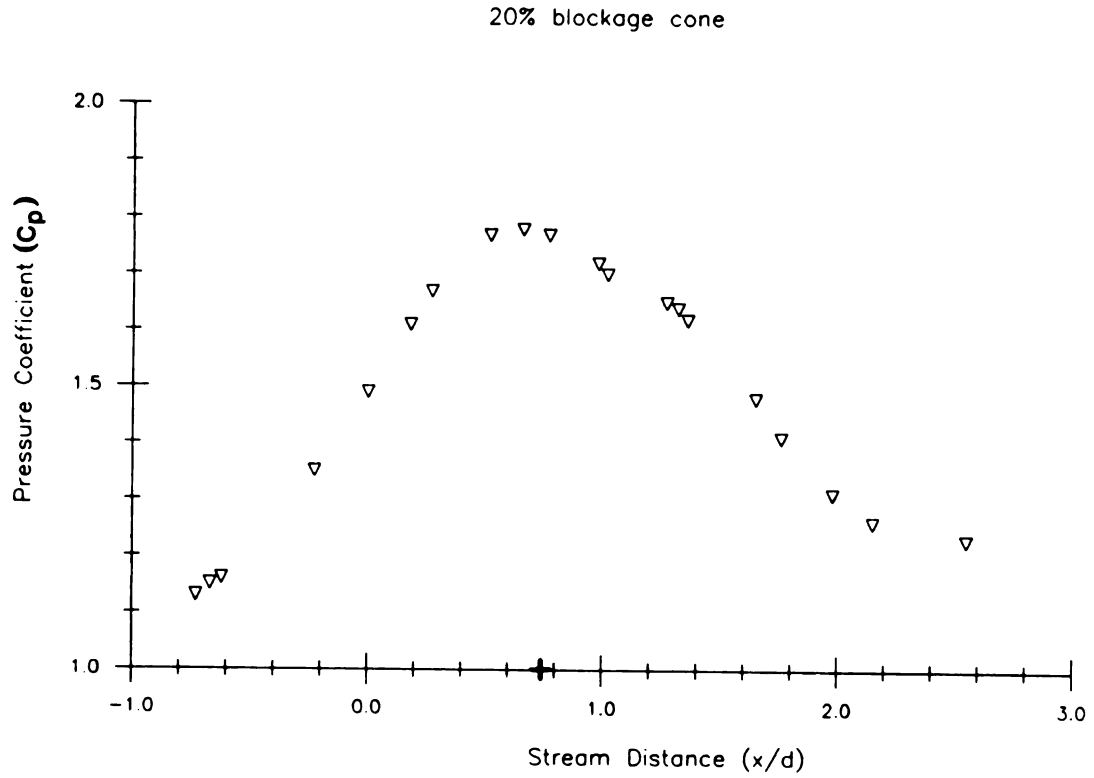
Figure 5.7 Streamwise Pressure Profiles for the 20% and 50% Blockage Cones.

blockage ratios. This was a trend that was also observed by Taylor and Whitelaw (1984) for disks of 25% and 50% blockage ratios. In the same study Taylor and Whitelaw observed the pressure minimum for a 25% blockage cone to be at an axial location of approximately 0.5 pipe diameters downstream of the base of the cone (Re = 3.89 x 10^4 based on annular velocity at the edge of cone and the cone diameter). This compares with the downstream location of 0.3 pipe diameters for the pressure minimum of the 20% blockage cone of the present investigation.

The pressure profiles also allow calculation of the effective annular area for the flow past the cone section and recirculation region where the flow passage is defined by the separation stream surface and the tube wall. The effective annular flow area was calculated using a simplified Bernoulli equation and assuming a uniform radial velocity profile. The control volume and calculations are presented in Appendix B. The effective annular flow area was calculated to be 0.018 m^2 for the 20% blockage cone and 0.0057 m^2 for the 50% blockage cone. This represents effective blockage ratios of 44% and 82%, respectively. This effective blockage ratio represents an increase of 64% for the 50% blockage cone and an increase of 120% for the 20% blockage cone. Taylor and Whitelaw (1984) and Winterfeld (1965) also observe this trend. The complete set of results is presented in Table 5.1.

The mean and rms velocity profiles in the axial direction for the 50% and 20% blockage cones are presented in Figures

Table 5.1 Width of Maximum Cross Sectional Area of Recirculation Region Aft of Bluff Bodies in Confined Flow

Author	Geometry	Radius[1]	Re
This Investigation	Confined cone – 45 deg., 20% blockage	0.74	1.7E5[3]
	Confined cone – 45 deg., 50% blockage	0.64	1.7E5
Taylor and Whitelaw (1984)	Confined disk – 25% blockage	0.62	3.5E4[2]
	Confined disk – 50% blockage	0.55	5.8E4
Winterfeld (1965)	Confined disk – 25% blockage	0.74	2.0E5[3]
	Confined disk – 4% blockage	0.84	2.0E5
	Confined cone – 90 deg., 25% blockage	0.64	2.0E5
	Confined cone – 90 deg., 4% blockage	0.72	2.0E5
	Confined cone – 45 deg., 25% blockage	0.58	2.0E5
	Confined cone – 45 deg., 4% blockage	0.60	2.0E5

Notes:

(1) radius of widest cross sectional area of recirculation region non-dimensionalized with cone or disk diameter

(2) based on annular velocity at edge of disk and diameter of disk

(3) based on approach velocity and confining tube diameter

5.8 and 5.9, respectively. The axial position of the measurement location for the spectral analysis is provided on all plots. For the 50% blockage cone the largest velocity value occurs at approximately 0.8 cone diameters downstream of the base of the cone. The 20% blockage cone has the largest velocity occurring at approximately 0.69 cone diameters downstream of the base of the cone. There is very good agreement on the inferred location of the widest part of the recirculation region between the velocity and pressure profiles. There is a 4% difference between the location of the largest pressure coefficient value and the largest non-dimensional velocity value for the 20% blockage cone and a 3% difference for the 50% blockage cone. It can be inferred that the effect of the streamline curvature on the axial velocity profile is minimal. That is, the largest velocity value closely corresponds to the region where the annular flow is most constricted.

The velocity rms plots for both blockage ratios suggest that there exists a fairly constant degree of flow unsteadiness near the edge and slightly downstream of the cone. Further downstream the velocity fluctuations continually increase. The velocity rms plot for the 20% blockage cone has the appearance of leveling off to a fairly constant value (except the value at $x/d = 1.9$) at locations downstream of $x/d = 1.5$. These plots demonstrate that there is a relatively large increase in the velocity fluctuations in the downstream regions of the recirculation region. It is inferred that this is caused by the motions of the
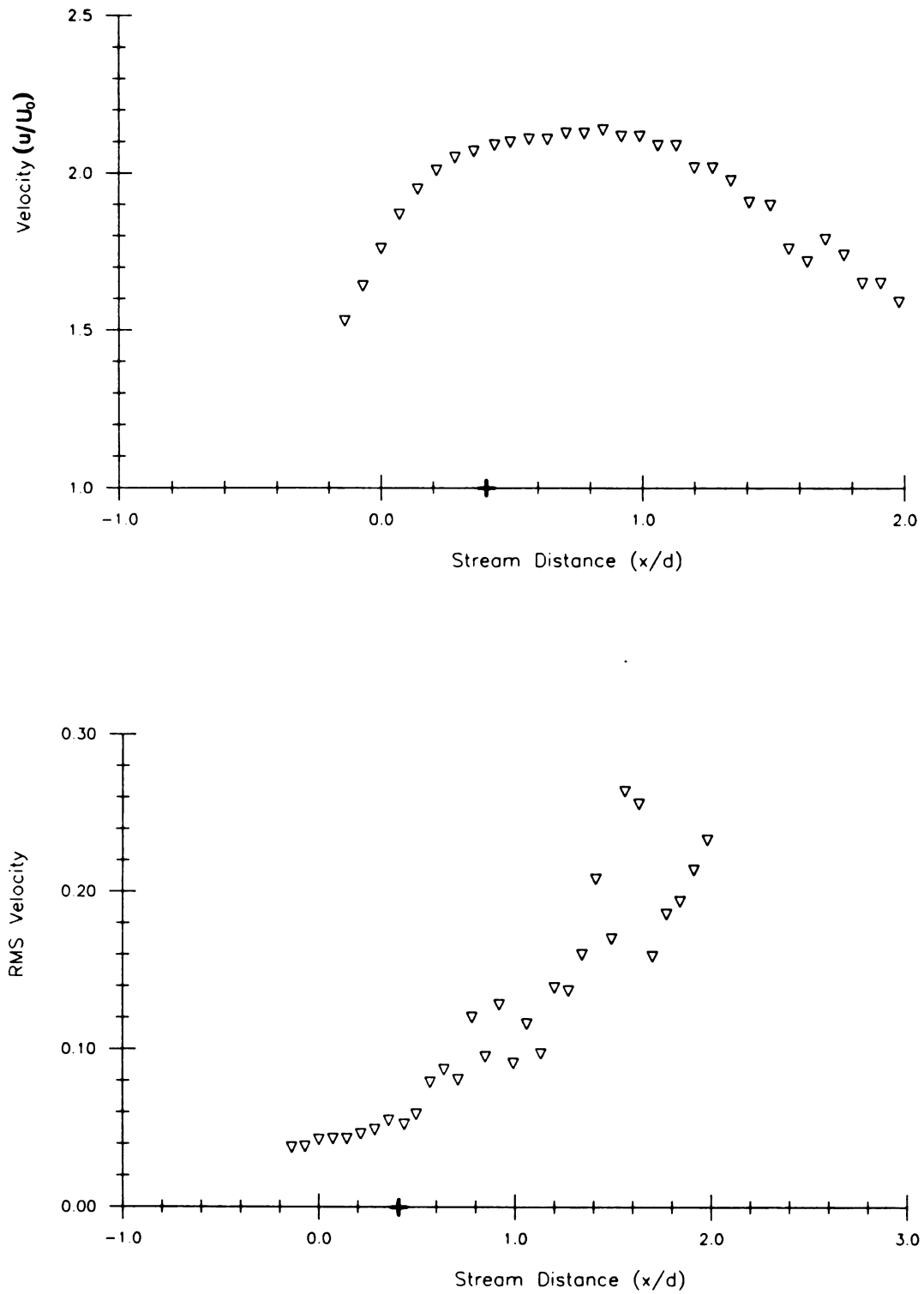
Figure 5.8   Streamwise Mean and   RMS Velocity Profiles for the 50%   Blockage Cone.
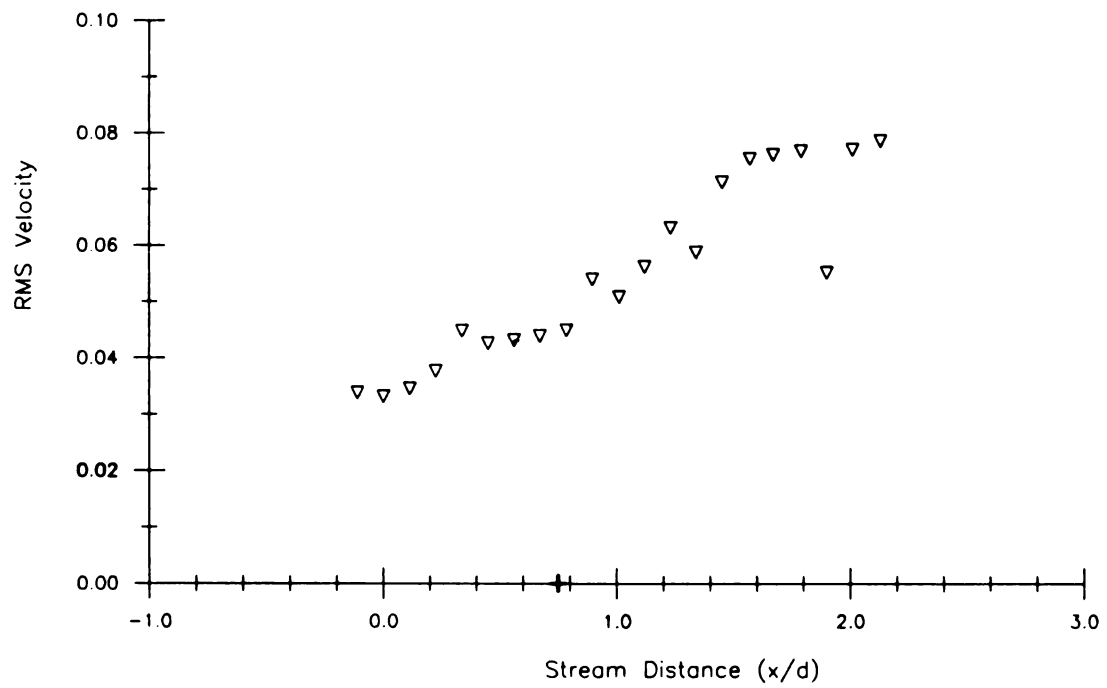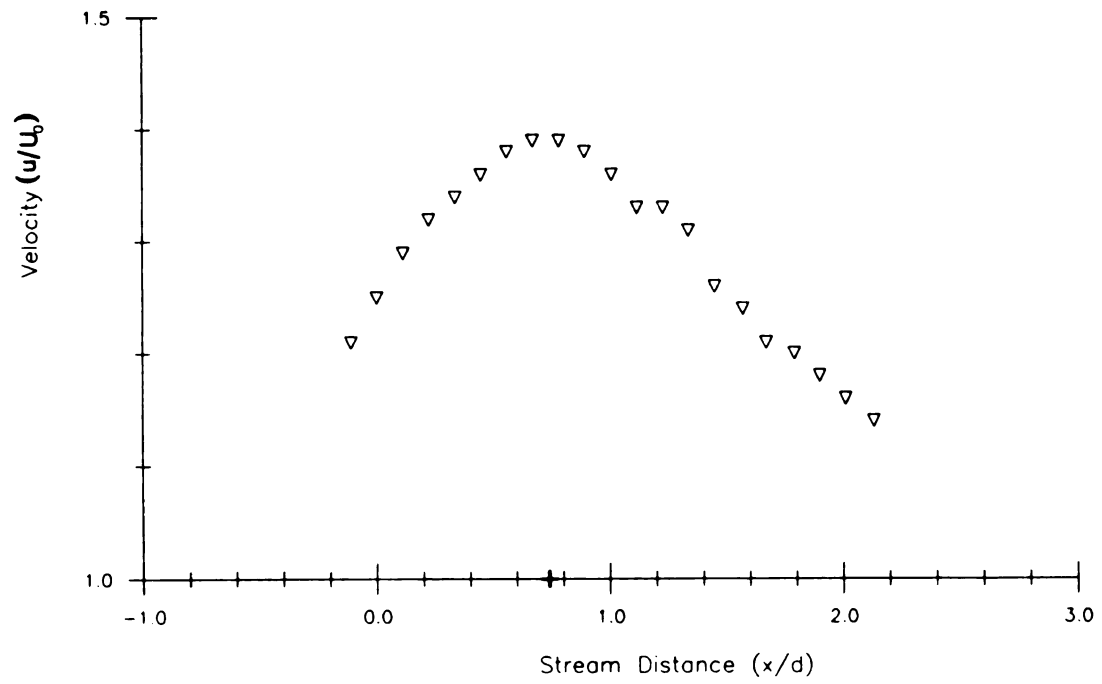
Figure 5.9 Streamwise Mean and RMS Velocity Profiles for the 20% Blockage Cone.

recirculation region. For both blockage ratios the measurement location for the spectral study is in an area of relatively low velocity fluctuations. The turbulence intensity at the measurement location is approximately 2.4% for the 50% blockage cone and 3.1% for the 20% blockage cone.

5.3. Results of Experiments Performed for
Determination of Probe Holder Effect

The pressure coefficient profiles, with and without the probe holding apparatus, are plotted for the 50% blockage cone; these data are presented in Figure 5.10. As mentioned in Section 4.1.4., the experiments for the determination of the probe holder effect were only performed on the 50% blockage cone. Although the comparative pressure measurements started at $x/d = 1.4$ and continued downstream, it can be inferred that the pressure, and thus the flow, at the hot-wire measurement location ($x/d = 0.4$) is not greatly affected by the presence of the probe holding apparatus. This is supported by the increasing agreement between the data sets of Figure 5.10 as x/d decreases. There is a 0.6% difference between the two pressure values at axial locations of $x/d = 1.4$. This increases to a high of 1.3% difference between the pressure values at $x/d = 1.82$ (slightly upstream of the location of the nose of the probe holding apparatus). The increasing offset between the two data sets may be attributed to the pressure deficit created by the fluid acceleration around the probe holding
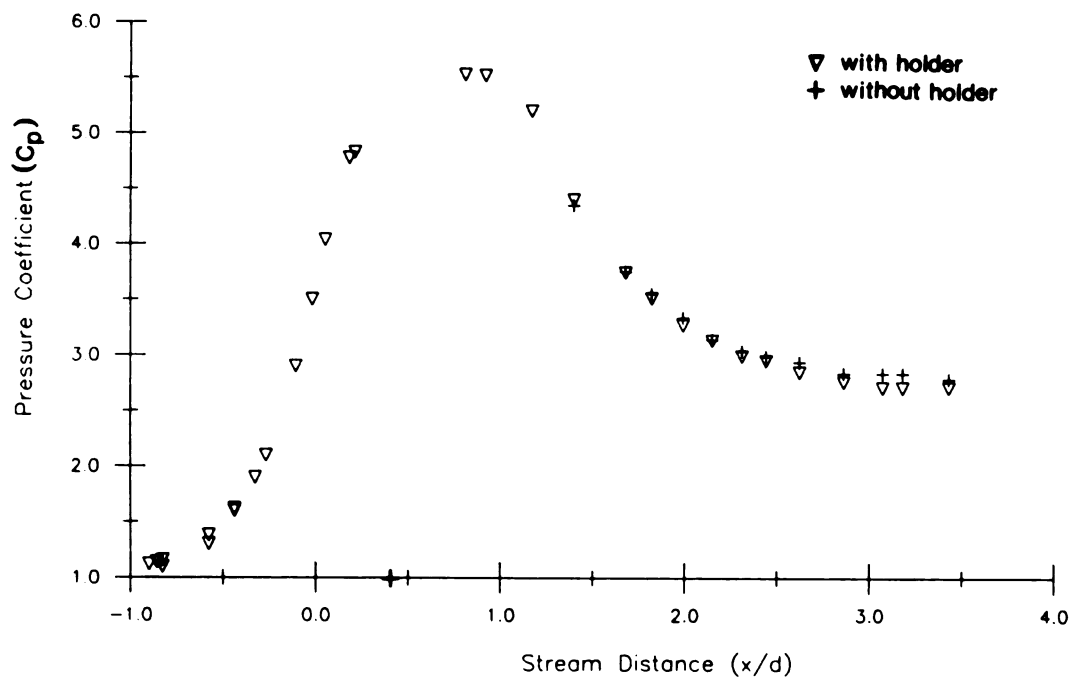
Figure 5.10 Streamwise Pressure Coefficient Profiles for the 50% Blockage Cone With and Without the Probe Holding Apparatus.

apparatus.

The results of the one-point LDA velocity measurements at the downstream location of x/d = 1.3 with and without the probe holding apparatus are presented in Table 5.2. The sampling conditions of the two data sets were the same except that the trigger level setting on the counter was higher for Data Set #2. The mean value of the velocity at the LDA measurement location is negative, thus revealing a region of reverse flow. This indicates that the LDA measurement location lies within the recirculation region (as was discussed in Section 2.2.).

For n statistically independent samples of a Gaussian distributed population, the uncertainty in the mean value ($\bar{\mu}$) is expressed as

$$[\bar{\mu}_S - \bar{\mu}_\infty] = \sigma_\infty \frac{\sqrt{n}}{n} \tag{5.4}$$

where μ_S represents the sample, μ_∞ represents the infinite population, and σ is the standard deviation. For the sample sizes listed in Table 5.2, the uncertainty in the mean velocity was estimated by

$$\sigma_S \frac{\sqrt{n}}{n} . \tag{5.5}$$

The mean velocity of Data Set #1 had an approximate uncertainty of 0.03 m/s. The uncertainty of the mean velocity of Data Set #2 was approximately 0.04 m/s.

Table 5.2 Mean Velocity From One-Point LDA Measurement With
and Without Probe Holding Apparatus

Data Set	Mean[3]	RMS[3]	Maximum	Minimum	Sample Size
#1[1]	-4.25	0.9727	-0.913	-6.95	512
	-4.13	0.9363	-0.68	-6.47	1024
	-4.24	0.945	-0.983	-6.69	1024
#1[2]	-4.16	0.9249	-0.225	-6.05	512
	-4.16	0.9487	-0.913	-6.67	1024
	-4.21	------	-0.733	-6.27	1024
#2[1]	-3.28	1.12	-0.99	-7.35	768
	-3.20	1.04	-1.05	-7.05	768
	-3.24	1.11	-0.85	-6.85	768
	-3.28	1.11	-0.85	-7.35	768
#2[2]	-3.07	1.046	-0.35	-6.85	768
	-3.03	0.989	-0.85	-7.35	768
	-3.06	1.1	-0.75	-7.35	768
	-3.06	1.033	-0.65	-6.85	768
	-3.23	1.118	-0.75	-7.35	768
	-3.15	1.059	-0.75	-----	768

Notes:

(1) data set taken with probe holding apparatus in position

(2) data set taken without probe holding apparatus in position

(3) units in m/sec

The results of Data Set #1, with and without the probe holding apparatus, reveal a negligible (approximately 0.7%) difference in the mean velocity values. The results of Data Set #2 show a comparatively larger (approximately 4%) difference in the mean velocity values with and without the apparatus present in the measuring section. These results imply that there is no significant change in the flow field of the recirculation region caused by the introduction of the probe holding apparatus into the measuring section.

Applying the LDA measurement technique provided the results shown in Table 5.2. The magnitude of the mean velocity values for Data Set #2 are significantly lower than those for Data Set #1. The reason for this difference is the setting of the trigger level on the counter. Any other contributing factors are not apparent. The purpose of the LDA measurement (to show the influence of the probe holding apparatus on an area of the recirculation region) is, however, addressed since the mean values of the velocity are minimally changed.

5.4. Results of the Spectral Analysis

An averaged power spectrum of ten blocks of data for each angular array was calculated for the hot-wire time series of Probes A and B (see Figure 4.5 for definition of probe lettering). The averaged power spectra for each angular array of Probe A for the 20% blockage cone are presented in Figure 5.11. Figure 5.12 contains the three averaged power spectra of Probe B for the 20% blockage cone. It is
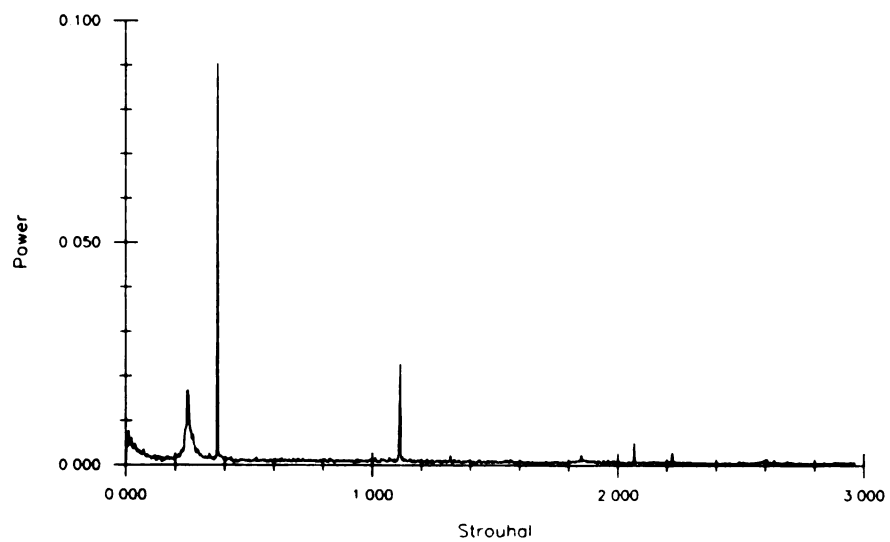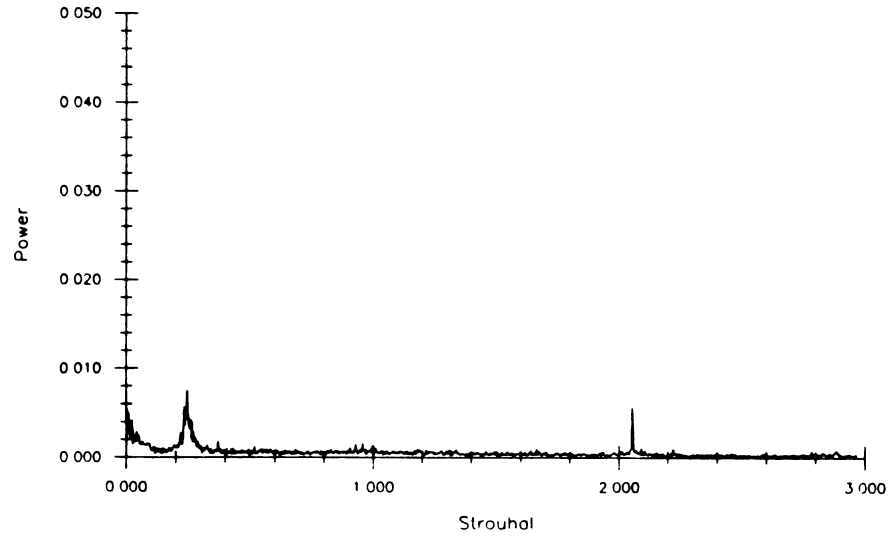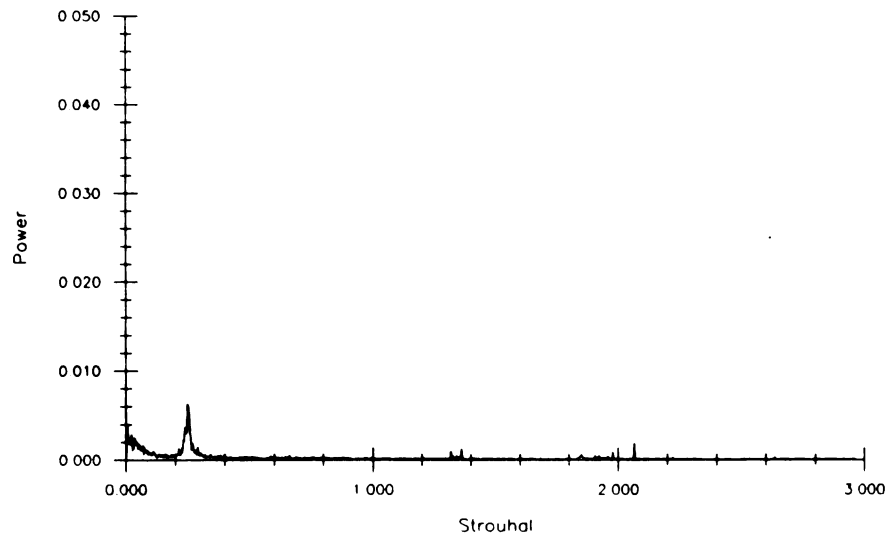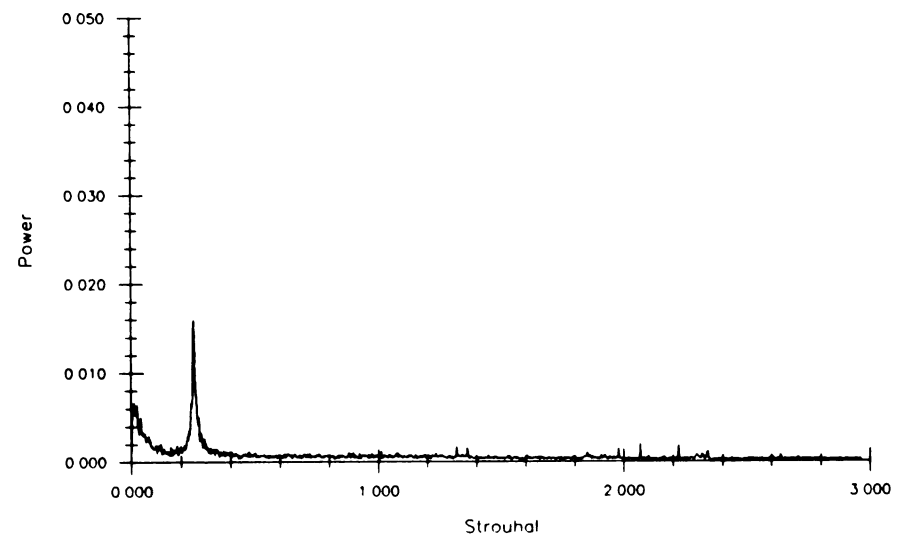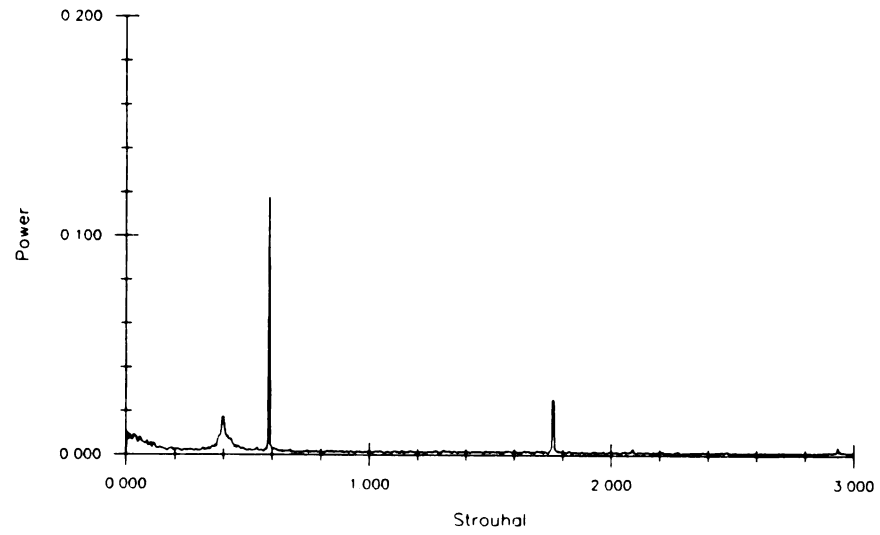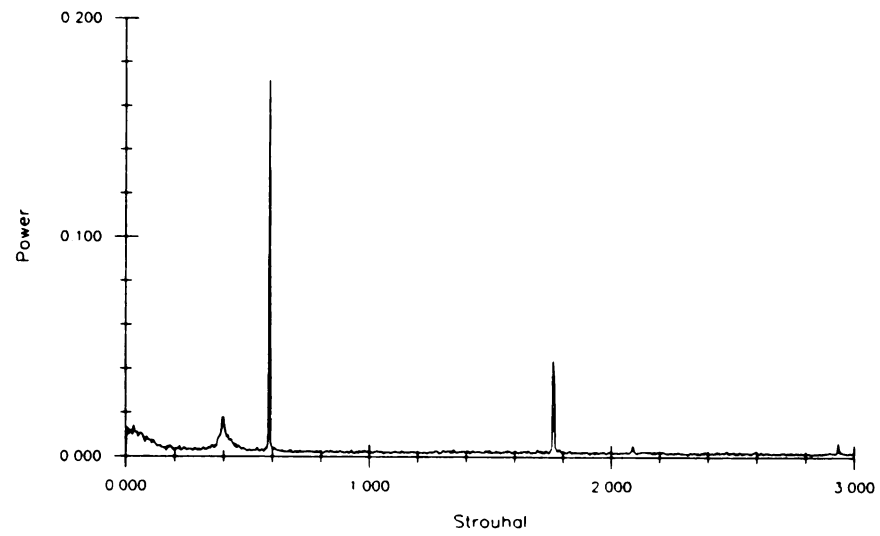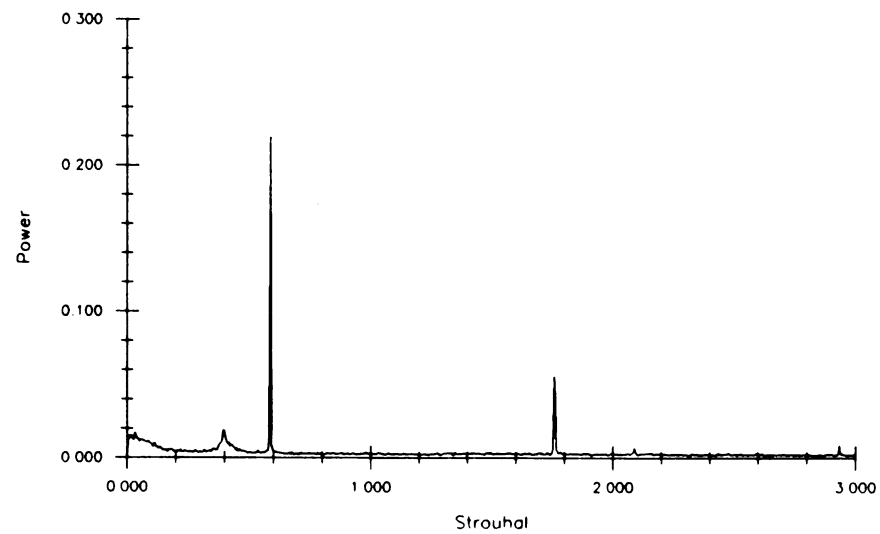
case 1
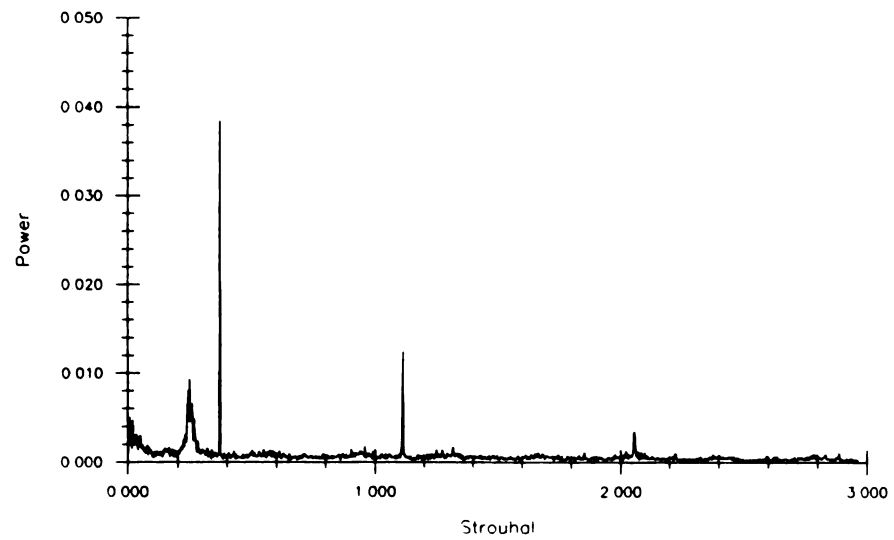
case 2
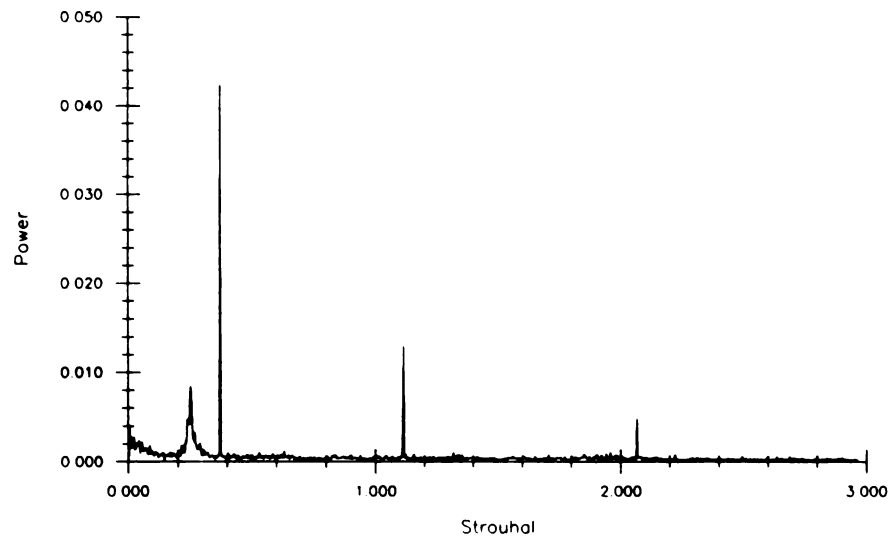
case 3

Figure 5.11   Averaged Power Spectrum of Each Angular Array
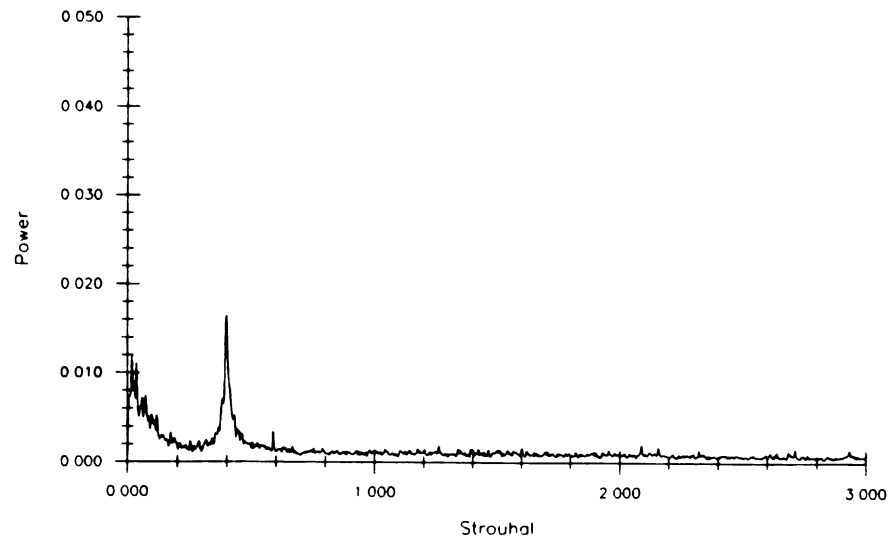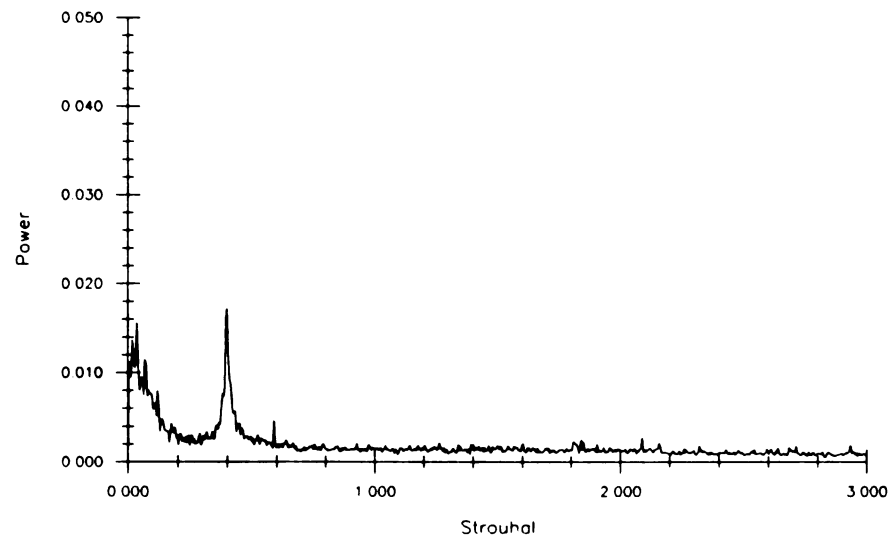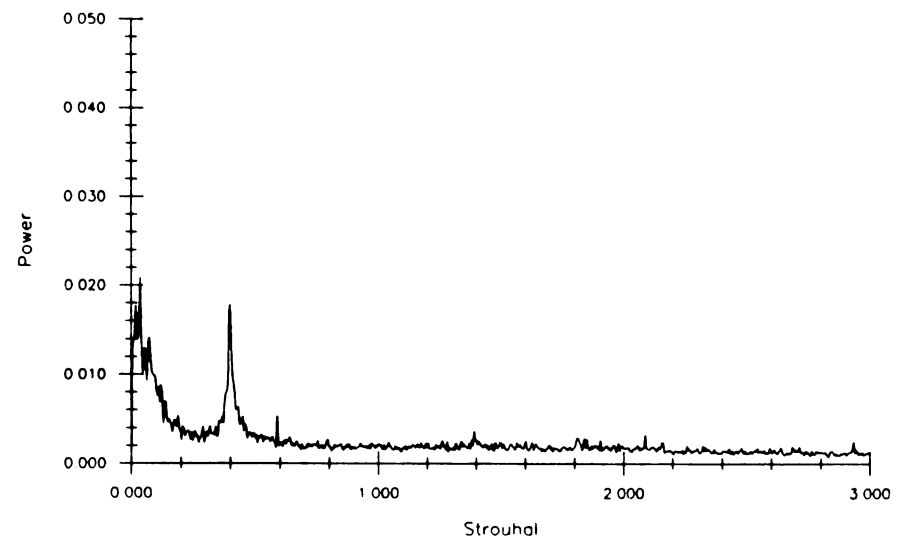of   Probe A for the 20% Blockage Cone.

case 1

case 2

case 3

Figure 5.12   Averaged Power Spectrum of Each Angular Array
of Probe B for the 20% Blockage Cone.

recognized that the averaged power spectra for the hot-wire time series of a probe at every azimuthal location at a given radial position should be equivalent. Comparing the averaged power spectra of Probes A and B it is clear that this is not the case. The large spikes at Strouhal numbers (as defined with the approach flow velocity and diameter of the cone base) of 0.37 and 1.11 for Probe A do not show up on the plots for Probe B. The spike at Strouhal number 2.06 for Probe A has a very small amplitude on the plot for Probe B. It is inferred that these spikes are caused by a mechanical vibration of the holder of Probe A. The peak at Strouhal number 0.25 occurs on all of the plots. The averaged power spectra of each angular array of Probe A for the 50% blockage cone are presented in Figure 5.13. Figure 5.14 contains the three averaged power spectra of Probe B for the 50% blockage cone. These plots show the same trends as those for the 20% blockage cone.

The seeming difference in the results of the power spectra between the two blockage ratios is shown to be due to predominant energy contributions at the same frequencies. This supports the supposition that the motions generating the spikes (as opposed to the initial peak) are mechanical in nature. The peak (at St = 0.40 for the 50% blockage cone and St = 0.25 for the 20% blockage cone) appears to be rather wide to be generated by a condition of mechanical resonance. It is inferred that this peak is associated with a standing wave in the flow system. This would account for the broad nature of the peak since there are no fixed

case 1

case 2

case 3

Figure 5.13   Averaged Power Spectrum of Each Angular Array
of Probe A for the 50% Blockage Cone.

case 1

case 2

case 3

Figure 5.14 Averaged Power Spectrum of Each Angular Array
of Probe B for the 50% Blockage Cone.

endpoints for the entire flow circuit associated with this standing wave (allowing slight variations of the wavelength). The wavelength of the standing wave is defined by

$$\lambda = a/f \qquad (5.6)$$

where   a = speed of sound

f = frequency of the wave.

Substituting known values of f and a, the wavelength is found to be about 9700 mm. This is approximately the circuit length of the flow system for the present investigation.

There are no peaks in the averaged power spectra plots that appear to correspond to any coherent motions of the recirculation region or vortex shedding from the cone. Because coherent motions do not dominate the unsteady flow field , the data processing technique of Fuchs et al (1979) can not be implemented.

6. SUMMARY AND CONCLUSIONS

The following summary statements and conclusions are supported by the results of this study:

1.) A topological evaluation of the surface streaking results on the base of the cone presents a logical distribution of singular points to explain the unexpected accumulation of lampblack fluid in a ring with a diameter slightly smaller that the base diameter of the cone. The ring is inferred to be a separation line for the radial outflow at the base of the cone. This flow is also inferred to reattach before joining the "through flow" at the sharp trailing edge of the cone.

2.) The axial location of the widest part of the recirculation region is 0.8 cone diameters downstream from the base of the 20% blockage cone and 0.67 cone diameters downstream from the base of the 50% blockage cone.

3.) The widest part of the recirculation region presented an effective blockage ratio of 44% for the 20% blockage cone and 82% for the 50% blockage cone.

4.) There is a reduction in the maximum cross sectional area of the recircultion region with increasing blockage ratio.

5.) There were no coherent motions of the recirculation region or vortex shedding from the cone observed at the blockage ratios of 0.20 and 0.50.

6.) The wake and the wall boundary layer meet before the end of the confining tube. Hence, vortical fluid exists over the entire diameter of the pipe sufficiently far downstream.

APPENDICES

APPENDIX A

APPENDIX A

Calculation of Flow Disturbance Caused by Piano Wire

The following analysis quantifies the flow disturbance produced by the piano wire used to stabilize the 50% blockage cone. Vortex shedding from a cylinder starts to occur at a Reynolds number of approximately 44. The Reynolds number of the flow around the piano wire (approximated by a cylinder of diameter 0.15 mm) is calculated to be 122. Therefore, vortices will be shed. The frequency of the vortex shedding from one side is calculated with the approach velocity, U_O, and the cylinder diameter, d, using the equation

$$fd/U_O = 0.2.$$

With an approach velocity of 12 m/s, the vortex shedding frequency is 1.6×10^4. Since the top of the cone section is 190 mm (1267 wire diameters) downstream of the piano wire, it is inferred that these disturbances created by the piano wire will die out before the top of the cone section is reached.

APPENDIX B

APPENDIX B

Calculation of the Effective Annular Flow Area

The effective annular area of the flow around the recirculation region was calculated using the control volume shown in Figure B.1. This area is defined as the area that is required to generate an equal mass flux at both Boundaries 1 and 2. The velocity, U, at Boundary 2 was calculated using a simplified form of the Bernoulli equation for a steady, incompressible, inviscid flow with a uniform axial velocity profile:

$$U_2 = \sqrt{U_1^2 + (2/\rho)(p_2 - p_1)} \qquad (B.1)$$

where ρ is the density and p is the pressure. The annular cross sectional area at Boundary 2 was calculated using the conservation of mass equation for steady flow of constant density, and a fixed control volume:

$$\int_{cs} (\vec{U} \cdot \hat{n}) \, dA = 0 \qquad (B.2)$$

where n is the outwardly directed unit vector normal to the control surface. The x component of this equation reduces to:
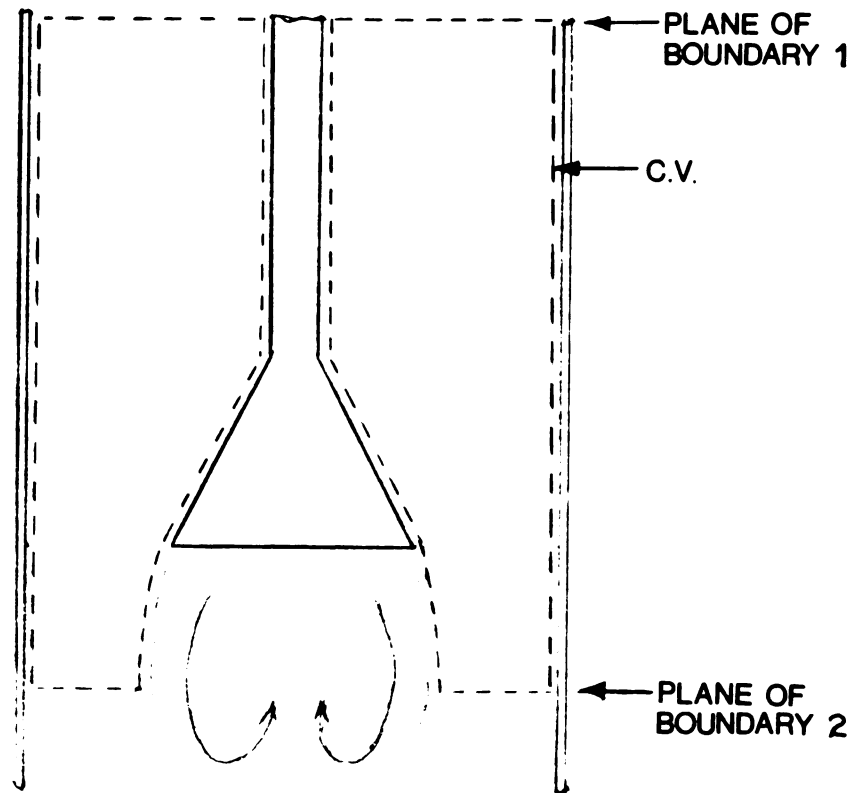
$$(U_2 A_2 = U_1 A_1). \qquad (B.3)$$

Figure B.1 Control Volume for Effective Annular Flow Area
Calculation.

Equation B.3 can be directly solved for the annular cross sectional area, A, at Boundary 2.

The radius, w, of the largest cross sectional area (approximated by a circle) can be found by subtracting A_2 (of equation B.3) from the cross sectional area of the pipe, A_O, and solving for w:

$$w = \sqrt{\frac{A_O - A_2}{\pi}} \qquad (B.4)$$

The quantity of equation B.4, non-dimensionalized by the cone diameter, is listed in Table 5.1.

LIST OF REFERENCES

LIST OF REFERENCES

Calvert, J.R. (1967): "Experiments on the Low-Speed Flow Past Cones," Jour. Fluid Mech., Vol. 27, pp. 273-289.

Carmody, T. (1964): "Establishment of the Wake Behind a Disk," Jour. of Basic Engineering, December 1964, pp. 869-883.

Durao, D.F.G. and Firmino, F.C. (1984): "Velocity Characteristics of the Flow Around Disks and Cones," Transactions of the ASME, Vol. 106, June 1984, pp. 167-171.

Durao, D.F.G. and Whitelaw, J.H. (1978): "Velocity Characteristics of the Flow in the Near Wake of a Disk," Jour. Fluid Mech., Vol. 85, Part 2, pp. 369-385.

Durrani, T.S., and Greated, C.A. (1977): Laser Systems in Flow Measurement, Plenum Press, New York

Foss, J.F. (1988): "Surface Selections and Topological Constraint Evaluations for Flow Field Analyses," submitted for publication to Jour. Fluid Mech.

Fuchs, H.V., Mercker, E., and Michel, U. (1979): "Large-Scale Coherent Structures in the Wake of Axisymmetric Bodies," Jour. Fluid Mech., Vol. 93, pp. 185-207.

Fujii, S., and Eguchi, K. (1981): "A Comparison of Cold and Reacting Flows Around a Bluff Body Flame Stabilizer," Jour. of Fluids Engineering, Transactions of the ASME, Vol. 103, pp. 328-334.

Fujii, S., Gomi, M., and Eguchi, K. (1978): "Cold Flow Tests of a Bluff-Body Flame Stabilizer," Jour. of Fluids Engineering, Transactions of the ASME, Vol. 100, pp. 323-333.

Humphries, W. and Vincent, J.H. (1976): "Near Wake Properties of Axisymmetric Bluff Body Flows," Appl. Science Res., Vol. 32, pp. 649-669.

Hunt, J.C.R., Abell, C.J., Peterka, J.A., and Woo, H. (1978): "Kinematical Studies of the Flows Around Obstacles; Applying Topology to Flow Visualization," Jour. Fluid Mech., Vol. 86, pp. 179-200.

Kamemoto, K., Oda, Y., and Aizawa, M. (1984):
"Characteristics of the Flow Around a Bluff Body Near a
Plane Surface," Bulletin of JSME, Vol. 27, No. 230, August
1984, pp. 1637-1634.

Lam, K.M., Ko, N.W.M., and Lau, K.K. (1986): "Wake and
Wake-Induced Shear Layer Excitation in an Annular Jet,"
Phys. Fluids, Vol. 29, No. 10, pp. 3121-3134.

Smith, R.H., and Wang, C. (1944): "Contracting Cones Giving
Uniform Throat Speeds," Jour. of the Aeronautical Sciences,
October 1944, pp. 356-360.

Taylor, A.M.K.P., and Whitelaw, J.H. (1984): "Velocity
Characteristics in the Turbulent Near Wakes of Confined,
Axisymmetric Bluff Bodies," Jour. Fluid Mech., Vol. 139, pp.
391-416.

Winterfeld, G. (1965): "On Processes of Turbulent Exchange
Behind Flame Holders," Tenth Symposium (Intl) on Combustion,
Combustion Institute, Pittsburgh, PA, pp. 1265-1275.

Xia, X.J., and Bearman, P.W. (1983): "An Experimental
Investigation of the Wake of an Axisymmetric Body With a
Slanted Base," Aeronautical Quarterly, Vol. 34, pp. 24-45.